Discovery of genes that modulate flavivirus replication in an interferon-dependent manner

Sarah Lesage[1,2]*, Maxime Chazal[1]*, Guillaume Beauclair[1,3], Damien Batalie[4], Elodie Couderc[1,5], Aurianne Lescure[6], Elaine Del Nery[6], Frédéric Tangy[7], Annette Martin[4], Nicolas Manel[8#] and Nolwenn Jouvenet[1#]

* These authors contributed equally

[#] corresponding authors

[1] Institut Pasteur, Virus Sensing and Signaling Unit, UMR3569 CNRS, Paris, France

[2] Université de Paris, Paris, France

[3] Université Paris-Saclay, CEA, CNRS, Institute for Integrative Biology of the Cell (I2BC), Gif-sur-Yvette, France

[4] Institut Pasteur, Molecular Genetics of RNA Viruses Unit, UMR3569 CNRS, Université de Paris, Paris, France

[5] Institut Pasteur, Insect-Virus Interactions Unit, Department of Virology, UMR2000 CNRS, Paris, France

[6] Institut Curie, PSL Research University, Department of Translational Research-Biophenics High-Content Screening Laboratory, Cell and Tissue Imaging Facility (PICT-IBiSA), Paris, France

[7] Institut Pasteur, Viral Genomics and Vaccination Unit, UMR3569 CNRS, Paris, France

[8] Institut Curie, PSL Research University, INSERM U932, Paris, France.

Short title: Modulation of flavivirus replication by interferon effectors

Summary

Establishment of the interferon (IFN)-mediated antiviral state provides a crucial initial line of defense against viral infection. Numerous genes that contribute to this antiviral state remain to be identified. Using a loss-of-function strategy, we screened an original library of 1156 siRNAs targeting 386 individual curated human genes in stimulated microglial cells infected with Zika virus (ZIKV), an emerging RNA virus that belongs to the flavivirus genus. The screen recovered twenty-one potential host proteins that modulate ZIKV replication in an IFN-dependent manner, including the previously known IFITM3 and LY6E. Further characterization contributed to delineate the spectrum of action of these genes towards other pathogenic RNA viruses, including Hepatitis C virus and SARS-CoV-2. Our data revealed that APOL3 acts as a proviral factor for ZIKV and several other related and unrelated RNA viruses. In addition, we showed that MTA2, a chromatin remodeling factor, possesses potent flavivirus-specific antiviral functions. Our work identified previously unrecognized genes that modulate the replication of RNA viruses in an IFN-dependent way, opening new perspectives to target weakness points in the life cycle of these viruses.

Author summary

The interferon (IFN) response, which is a powerful arm of the antiviral immune program, protects cells from invading viral pathogens by transcriptionally inducing the expression of interferon-stimulated genes (ISGs). ISGs effectively establish the antiviral state by directly blocking the viral life cycle by targeting specific stages of replication. Some ISGs are specific to a virus or a viral family, while others are broad-spectrum. Identifying which ISGs exert antiviral function against which virus is crucial because it enables the subsequent understanding of weakness points in the life cycle of viruses. Using a loss-of-fonction screening strategy, we investigated the ability of 386 unique ISGs to inhibit the replication of Zika virus (ZIKV), a virus that recently emerged in the Pacific and the Americas. Using this approach, we identified novel modulators of ZIKV replication in IFN-treated human cells. Our work contributes to a better understanding of the molecular basis behind the complexity the antiviral program. Furthermore, taking advantage of naturally occurring viral inhibitors may be an effective strategy for the development of novel drugs that activate, amplify or mimic their action.

Introduction

Viruses are high on the list of global public health concerns, as illustrated by recent epidemics caused by Ebola, Zika (ZIKV) and Nipah viruses, as well as by the ongoing SARS-CoV-2 pandemic. The vast majority of these emerging RNA viruses have zoonotic origins and have recently crossed host species barrier [1]. In order to establish itself in a host species, one of the first and most restrictive barriers that a virus needs to overcome is the antiviral innate immune system. This response has evolved to rapidly control viral replication and limit virus spread *via* detection of viral nucleic acids by pathogen recognition receptors (PRRs) [2]. These PRRs can be membrane-associated, such as Toll-like receptor (TLRs), or cytosolic, such as retinoic acid inducible gene I (RIG-I)-like receptor (RLRs). Upon binding to viral nucleic acids, these PRRs interact with adaptor proteins and recruit signaling complexes. These events lead to the expression of type I interferons (IFNs). Secreted IFNs will then bind to their heterodimeric receptor (IFNAR1/IFNAR2) and activate the canonical JAK/STAT pathway in infected and surrounding cells. This activation triggers the assembly of the interferon-stimulated gene 3 (ISGF3) complex (composed of STAT1, STAT2 and IRF-9 proteins), which subsequently induces the expression of up to approximately 2000 IFN-stimulated genes (ISGs) [3,4], effectively establishing the antiviral state. ISGs comprise a core of genes that are induced at high levels essentially in all cell types, as well as cell-type specific genes that are the result of transcriptome remodeling [5,6], highlighting the importance of studying ISGs in relevant cell types. Some of these ISGs have been well characterized. They directly block the viral life cycle by targeting specific stages of virus replication, including entry into host cells, protein translation, replication or assembly of new viral particles [3,7]. Some ISGs are specific to a virus or a viral family, while others are broad-spectrum. They can also be negative or positive regulators of IFN signaling and thus facilitate, or not, the return to cellular homeostasis. However, the contribution of most ISGs to the antiviral state remains poorly understood.

Over the last decades, flaviviruses have provided some of the most important examples of emerging or resurging diseases, including ZIKV, dengue virus (DENV), Yellow fever virus (YFV) and West Nile virus (WNV) [8]. These flaviviruses are arthropod-borne viruses transmitted to vertebrate hosts by mosquitoes. They cause a spectrum of potentially severe diseases including hepatitis, vascular shock syndrome, encephalitis, acute flaccid paralysis, congenital abnormalities and fetal death [8]. They are now globally distributed and infect up to 400 million people annually. Lesser-known flaviviruses are beginning to emerge in different parts of the world, as illustrated by the recent incursion of Usutu virus (USUV) in the Mediterranean basin [9].

ZIKV was isolated in 1947 in a macaque from the Zika Forest in Uganda [10]. For decades, it remained in Africa and Asia where it sparked local epidemics characterized by a mild self-limiting disease in humans. In recent years, Asian lineage viruses have emerged as a global public health threat with widespread epidemics in the Pacific Islands and Americas, where over 35 countries have reported local transmission in 2016. An estimated 1 million individuals were affected by ZIKV in Brazil in 2015-16. Infection by ZIKV has been linked to several neurological disorders, including Guillain-Barré syndrome (GBS),

96 meningoencephalitis, myelitis and congenital microcephaly, fetal demise and abortion [10]. Children
97 exposed to ZIKV in utero may present neurocognitive deficits, regardless of head size at birth. ZIKV
98 infection is now identified as a sexually-transmitted illness as well [11]. As all flaviviruses, ZIKV is an
99 enveloped virus containing a positive-stranded RNA genome of ~11 kb. Upon viral entry, the viral
100 genome is released and translated by the host cell machinery into a large polyprotein precursor. The
101 latter is processed by host and viral proteases into three structural proteins, including C (core), prM
102 (precursor of the M protein) and E (envelope) glycoproteins, and seven non-structural proteins (NS)
103 called NS1, NS2A, NS2B, NS3, NS4A, NS4B and NS5 [8]. The structural proteins constitute the viral
104 particle, while NS proteins coordinate RNA replication, viral assembly and modulate innate immune
105 responses.
106 The importance of IFN signaling in mediating host restriction of ZIKV is illustrated by the severe
107 pathogenicity in IFNAR1-/- and STAT2-/- but not in immunocompetent mice [12–14]. Moreover, the
108 Zika strain that is responsible for the recent epidemics has accumulated mutations that increase
109 neurovirulence via the ability to evade the immune response [15]. Microglial cells, which are the resident
110 macrophages of the brain, represent ZIKV targets and potential reservoirs for viral persistence [16].
111 Moreover, they may play a role in ZIKV transmission from mother to fetal brain [17] and affect the
112 proliferation and differentiation of neuronal progenitor cells [18]. In order to comprehend the molecular
113 bases behind the efficacy of the IFN response to ZIKV replication, we set up a high throughput assay to
114 identify genes that are modulating viral replication in human microglial cells (HMC3) stimulated with
115 IFN.
116

117 ## Results

118 ### A loss of function screen identified genes modulating ZIKV replication in IFN-stimulated
119 human microglial cells

120 We first performed pilot experiments to determine the feasibility of conducting large-scale loss-of-
121 function studies to identify novel genes regulating ZIKV replication in stimulated HMC3 cells. Five
122 hundreds cells were seeded in 384-well microplates on day 1, transfected with individual siRNA 6 hours
123 later, treated with IFNα2 at day 2, infected with ZIKV at day 3 and fixed 24 hours later (Fig. 1A).
124 Percentages of infected cells were determined by confocal analysis by measuring the number of cells
125 expressing the viral E protein, using the pan-flavivirus anti-E antibody 4G2 (Fig. 1A). Nuclei were
126 identified with DAPI staining for imaging and segmentation purposes. We optimized IFNα2
127 concentration and viral multiplicity of infection (MOI) to obtain a significant decrease of E-positive
128 cells upon IFNα2-treatment (Fig. S1A). We used siRNAs targeting IFNAR1, which are expected to
129 neutralize IFN signaling, as positive controls (Fig. S1A). siRNAs against IFITM3, an ISG known to
130 potently inhibit ZIKV replication in several human cell lines and primary fibroblasts [19,20], were used
131 as additional positive controls (Fig. S1A). Negative controls were non-targeting siRNAs. As expected,

132 in the presence of siRNAs targeting IFNAR1, IFN signaling was neutralized and the level of infection
133 was almost rescued to the level of non-treated cells (Fig. S1A). In cells silenced for IFITM3 expression,
134 the number of infected cells was partly restored to the level of non-treated cells (Fig. S1A). Such partial
135 rescue was expected since the antiviral state requires the concerted action of numerous ISGs [21]. These
136 data also revealed that IFITM3 is a potent anti-ZIKV ISG in microglial cells.

137 We scaled up the experiment by screening an arrayed library containing 1158 siRNAs targeting 386
138 human genes (Table S1). These genes were selected based on a gene signature defined by clustering and
139 correlation of expression with MX1, a well-described ISG, in a dataset of gene expression in primary
140 human $CD4^+$ T cells (Cerboni et al., in preparation). 36% of the identified genes overlapped with
141 previous ISG libraries [21,22], ensuring that the screen would be simultaneously capable of identifying
142 expected positive hits and find new genes of interest. To overcome potential off-target effect and a
143 limited efficacy of transcript knockdown, each gene was targeted by 3 different siRNAs. Numerous
144 siRNAs targeting IFNAR1 and IFNAR2 were used as positive controls. Negative controls were non-
145 targeting siRNAs. Transfection efficiency was evaluated using siRNAs against KIF11, a protein
146 essential for cell survival [23]. The same experimental protocol than in small-scale experiments was
147 applied (Fig. 1A). Three images were acquired per condition with an INCell2200 automated wide-field
148 system. The mean cell count and the percentages of infected cells were extracted from quantification.
149 The screen was performed in duplicate.

150 For quality control purposes, we first compared the number of cells in each well in the 2 replicates.
151 We observed an expected distribution of the number of cells in 3 fields with a median close to 1000
152 cells per well for the two replicates (Fig. S1B). The number of cells per condition was slightly higher in
153 the first replicate than in the second one. However, the R^2 coefficient of determination of the linear
154 regression was close to 0.7 (Fig. S1C), indicating that the reproducibility of the experiment was correct.
155 As expected [23], siRNAs against KIF11 were lethal, validating the transfection protocol (Fig. S1B, C).
156 The 2 screens were first analyzed by taking into consideration the intensity of the E signal per cell. The
157 number of cells expressing the viral protein E distributed as predicted, with a median close to 15% for
158 the 2 screens (Fig. S1D). As expected from pilot experiments (Fig. S1A), siRNAs targeting IFNAR-1
159 and -2 rescued ZIKV replication in IFN-treated cells (Fig. S1D, E). The reproducibility of the infection
160 status of the cells between the 2 screens, with a R^2 greater than 0.8, was satisfactory (Fig. S1E). The
161 data were then analysis using a second approach that identified infected cells based on the E expression
162 independently of the intensity of the signal. The 2 methods identified similar number of infected cells
163 (Fig. S1F). Results were expressed as robust Z-scores for each siRNA (Fig. 1B, C). Genes were defined
164 as hits when at least two over three of their robust Z scores had an absolute value superior to 2 in the
165 two replicates, in at least one of the analysis. The screen identified 9 antiviral genes and 12 proviral ones
166 (Fig. 1D). Some hits were previously described as modulators of ZIKV replication, such as IFITM3
167 [19,20] and LY6E [24], thus validating our loss-of-function screening approach. These twenty-one hits
168 were selected for further validation.

169 IFNα2-treated HMC3 cells were transfected with pool of 3 siRNAs against each candidate, and not
170 by individual ones as in the primary screening. Twenty-four hours post-ZIKV infection, intracellular
171 viral RNA production was quantified by RT-qPCR and the number of cells positive for the viral protein
172 E was assessed by flow cytometry analysis. The same samples were used to assess the efficacy of the
173 siRNAs. RT-qPCR analyses revealed that 15 out of the 21 siRNA pools were reducing the expression
174 of their respective targets in IFN-treated cells (Fig. S1G). mRNAs levels of C1R, XCL1, GBP3, NADK,
175 C22orf39 and RUBCN were below the detection limit in IFNα2-treated HMC3 (Fig. S1G). These genes
176 were thus excluded from further anaysis. Reduced expression of IRF9, IFITM3, MTA2 and GPD2
177 significantly enhanced both viral RNA yield and the number of infected cells as compared to IFNα2-
178 treated cells transfected with control siRNAs (Fig. 1E and F). Both IRF9, which belongs to the ISGF3
179 complex [25], and IFITM3 [26] are well-known broadly-acting IFN effectors. The activities of MTA2
180 have, so far, not been linked to antiviral immunity. MTA2 is a component of the nucleosome remodeling
181 deacetylase NuRD complex, which exhibits ATP-dependent chromatin remodeling activity in addition
182 to histone deacetylase activity [27]. Ten times more viral RNA copies were recovered in cells silenced
183 for MTA2 expression than in control cells (Fig. 1E) and four times more cells were positive for the viral
184 E protein (Fig. 1F). These effects were comparable to the ones induced by IFNAR1 silencing (Fig. 1E
185 and F). Transfection with siRNA against the other 3 antiviral candidates (PXK, NMI and IFI16) had no
186 significant effect on ZIKV replication in these assays (Fig. 1E and 1F), suggesting that they may be
187 false positive candidates. Reducing the expression of LY6E, ISG15 and APOL3 significantly decreased
188 both viral RNA production and the number of cells positive for the E protein (Fig. 1G and 1H), validating
189 the pro-viral activities of these 3 candidates. The pro-viral function of USP18 and NAPA were also
190 validated since reducing their expression led to a significant reduction of the number of infected cells
191 as compared to control cells (Fig. 1H). Reduced expression of ISG20 or CCND3 had no significant
192 effect on ZIKV replication (Fig. 1G and 1H). IRF2, which was identified as a pro-viral hit by the screen,
193 behaved like an antiviral gene in the validation experiments (Fig. 1G). Together, these experiments
194 validated the antiviral function of IRF9, IFITM3, MTA2 and GPD2 and the pro-viral function of LY6E,
195 USP18, ISG15, APOL3 and NAPA in IFNα2-treated HMC3 cells infected with ZIKV.
196
197 **Effect of a selection of candidate genes on HCV and SARS-CoV-2 replication**
198 We next explored the ability of 10 candidate genes (IRF9, IFITM3, MTA2, GPD2, LY6E, USP18,
199 ISG15, APOL3, GBP3 and NAPA) to modulate the replication of two other pathogenic RNA viruses:
200 Hepatitis C virus (HCV) and Severe Acute Respiratory Syndrome Coronavirus 2 (SARS-CoV-2), which
201 are, respectively, related and unrelated to ZIKV. HCV, which is a member of the Hepacivirus genus
202 within the *Flaviviridae* family, has a tropism for hepatocytes. SARS-CoV-2 belongs to the
203 *Coronaviridae* family and has a tropism for pneumocytes and enterocytes.

204 HCV infections were conducted in hepatoma Huh-7.5 cells, which support well viral replication [28].
205 Huh-7.5 cells are unable to induce IFN expression since they express an inactive form of RIG-I [29] but
206 they possess an intact JAK/STAT pathway and do thus respond to IFN treatment [30]. RT-qPCR
207 analyses revealed that 8 out 10 siRNA pools efficiently reduced the expression of their respective targets
208 in stimulated Huh-7.5 cells (Fig. S2A). Since LY6E and APOL3 mRNA levels were under the limit of
209 detection of the assays in IFNα2-treated Huh-7.5 cells (Fig. S2A), they were excluded from further
210 analysis. As expected, reduced expression of IFNAR and IRF9 significantly enhanced HCV RNA yield
211 and the production of infectious particles in IFNα2-treated Huh-7.5 cells, as compared to control cells
212 (Fig. 2A, B). Reduced expression of IFITM3, MTA2 or GPD2, which significantly enhanced ZIKV
213 replication in HCM3 cells (Fig. 1E, F), did not affect HCV RNA production (Fig. 2A). However,
214 surprisingly, their reduced expression triggered a significant decrease in the release of infectious HCV
215 particles as compared to control cells (Fig. 2B). This suggests that they might favor a late stage of HCV
216 replication cycle. RT-qPCR analysis and titration assays identified USP18 and ISG15 as pro-HCV
217 factors in IFNα2-treated Huh-7.5 cells (Fig. 2C, D), validating previous results [31–34]. Of note, HCV
218 RNA production and infectious particle release were significantly increased in cells with reduced NAPA
219 levels (Fig. 2C, D), suggesting that NAPA may exert an antiviral effect on HCV, while it was not the
220 case for ZIKV (Fig. 1G, H).
221 SARS-CoV-2 replication was assessed in A549 alveolar epithelial cells expressing the viral receptor
222 ACE2 (A549-ACE2) by RT-qPCR and flow cytometry analysis using an antibody against the viral
223 protein Spike (S). Of note, silencing GBP3 in A549-ACE2 cells triggered cell death. RT-qPCR analyses
224 showed that all siRNA pools were reducing the expression of their respective targets in stimulated A549-
225 ACE2 cells (Fig. S2B). These analyses revealed the ability of IRF9 to act as an anti-SARS-CoV-2 gene
226 (Fig. 2E, F). Unexpectedly, GPD2 and IFITM3, which we identified as genes possessing anti-ZIKV
227 activities (Fig. 1), tended to behave like pro-viral genes in the context of SARS-CoV-2 infection (Fig.
228 2E and 2F). Viral RNA yields decreased significantly in cells silenced for USP18, ISG15 and NAPA
229 expression, as compared to cells transfected with control siRNAs (Fig. 2G), suggesting that these 3
230 genes promote viral replication in stimulated A549-ACE2 cells. By contrast to what we observed in
231 ZIKV infected cells (Fig. 1G, H), LY6E seemed to restrict SARS-CoV-2 (Fig. 2H). These results are in
232 accordance with a recent report [35]. Reducing MTA2 or APOL3 expression did not affect SARS-CoV-
233 2 replication.
234 These results suggest that some genes are broadly-acting IFN effectors, such as IRF9 and ISG15.
235 Other genes appeared to have evolve modulatory function toward a specific viral family or genus, such
236 as APOL3 and MTA2. Finally, some genes, including LY6E, IFITM3 and GPD2, exhibited opposite
237 modulatory functions towards different viral species.
238
239 **ZIKV, DENV-2, WNV, VSV and MeV, but not MVA, require the expression of APOL3 for**
240 **optimal replication in IFN-treated cells**

241 LY6E, ISG15 and APOL3 exhibited significant pro-ZIKV activities in stimulated cells, as measured
242 by cell-associated viral RNA levels (Fig. 1G) and percentage of E-positive cells (Fig. 1H). Among these
243 3 genes, APOL3 is the least described and was thus selected for further characterization. APOL3 is one
244 of the 6 members of the apolipoprotein L gene family. Apolipoproteins are typically associated with the
245 transport of lipids in the organism and were originally described as members of the high-density
246 lipoprotein family, which are involved in cholesterol transport [36]. In human cells, the expression of
247 the 6 members of the APOL gene family are up-regulated by multiple pro-inflammatory signaling
248 molecules, including IFNs and TNFα [36,37]. These regulations suggest a link between APOL proteins
249 and the innate immune system. siRNA targeting APOL2, APOL3, APOL4, APOL5 and APOL6 were
250 present in our library (Table S1). Among these 5 APOLs, only APOL3 was identified as a facilitator of
251 ZIKV infection by our screen (Fig. 1). We decided to test the ability of APOL1 to modulate ZIKV
252 replication since it was previously identified in a high-throughput overexpression screen as an ISG able
253 to increase YFV infection in *STAT1*$^{-/-}$ fibroblasts and Huh-7cells [21].
254 Analysis of mRNA levels of APOL1 and APOL3 revealed that the genes were upregulated by
255 IFNα2 treatment in HMC3 cells (Fig. 3A). Both genes thus qualify as genuine ISGs in these cells. The
256 implication of APOL1 and APOL3 in ZIKV replication was investigated using loss-of-function
257 approaches. siRNA-silencing reduced the levels of APOL1 and APOL3 mRNAs by ~80% and ~85%,
258 respectively, when compared to cells expressing scrambled control siRNAs (Fig. 3B). USP18, which is
259 known to negatively regulates the JAK-STAT pathway, and, as such, is a broad-spectrum pro-viral
260 factor [38], was identified during our screen as a pro-ZIKV candidate in HMC3 cells (Fig. 1D). Since
261 its pro-ZIKV function was validated in our system (Fig. 1H), siRNAs specific for USP18 were used as
262 positive controls. siRNA-silencing reduced the abundance of USP18 mRNAs by ~80% when compared
263 to cells expressing control siRNAs (Fig. 3B). Viral replication was assessed by flow cytometry by
264 measuring the number of cells positive for the viral protein E in cells silenced for APOL1, APOL3 or
265 USP18, treated or not with IFNα2. Since ZIKV is sensitive to IFNα2-treatment (Fig. S1A), higher MOIs
266 were used in IFNα2-treated cells than in untreated ones to compensate for its antiviral effects. As
267 expected (Fig. 1H), reduced expression of USP18 significantly decreased the number of IFN-treated
268 cells positive for the viral protein E, as compared to cells transfected with control siRNAs (Fig. 3C).
269 Extinction of APOL1 and APOL3 resulted in a modest, but reproducible, decrease in the number of E-
270 positive HMC3 cells pre-treated with IFNα2 (Fig. 3C). A pro-viral effect of APOL1 was also observed
271 in unstimulated cells (Fig. 3C). The efficacy of the siRNAs against APOL1 and USP18 were further
272 validated by Western Blot analysis using specific antibodies (Fig. 3D). APOL3 levels in cell lysates
273 could not be assessed due to the lack of available antibodies. Levels of expression of the viral proteins
274 NS5 and E were slightly decreased in IFNα2-cells expressing reduced levels of APOL1 or APOL3,
275 compared to control cells (Fig 3D). Together, these results suggest that ZIKV requires the expression of
276 APOL1 and APOL3 for optimal replication in HMC3 cells. By contrast to APOL1, the pro-viral action

277 of APOL3 was dependent on IFNα2-treatment.

278 To ensure that the APOL1- and APOL3-mediated modulation of viral replication was not restricted
279 to HMC3 cells, silencing experiments were performed in ZIKV-infected human podocytes treated or
280 not with IFNα2. Podocytes are physiologically relevant for ZIKV infection since viral RNA was
281 detected in kidneys of infected patients [39]. Assessing the mRNA abundance of APOL1 and APOL3
282 by RT-qPCR analysis of cells treated or not with IFNα2 revealed that both genes qualify as ISGs in
283 podocytes (Fig. 3E). siRNA-mediated silencing of APOL1, APOL3 and USP18 was efficient in
284 podocytes (Fig. 3F). Reduced expression of APOL1 or APOL3 resulted in a significant decrease of the
285 percentage of infected cells in IFNα2-treated podocytes, but not in unstimulated cells (Fig. 3G). Western
286 blot analysis performed in IFNα2-treated podocytes revealed that cells expressing little APOL1/3 were
287 producing less viral proteins than controls cells (Fig. 3H), confirming the pro-ZIKV activity of the two
288 APOLs. These data revealed that APOL3 and APOL1 facilitate the replication of ZIKV in podocytes
289 treated with IFNα2.

290 We tested whether APOL1 and APOL3 were active against DENV-2 or WNV, which are mosquito-
291 borne flaviviruses closely related to ZIKV. HMC3 cells were treated or not with IFNα2 and the MOIs
292 were adapted to the IFNα2 treatment. Flow cytometry analysis using anti-E antibodies revealed that
293 both DENV-2 and WNV replication were significantly decreased in IFNα2-treated cells silenced for
294 APOL1 or APOL3 expression (Fig. 3I). Reducing APOL1 and APOL3 expression in non-treated cells
295 also significantly reduced WNV replication (Fig. 3I). Thus, APOL1/3 may well have flavivirus genus-
296 specific proviral activities since they seems to contribute to ZIKV, WNV and DENV replication (Fig.
297 3C, D, G, H and I) but not to SARS-CoV-2 replication (Fig. 2G, H). To further delineate the spectrum
298 of action of these two genes towards other viruses, we tested the effect of APOL1/3 silencing on the
299 replication of Vesicular Stomatitis virus (VSV) and Measles virus (MeV), which are negative-strand
300 RNA viruses belonging to the *Rhabdoviridae* and *Paramyxoviridae* families, respectively. Experiments
301 were performed with a MeV strain modified to express GFP [40]. We also included in the analysis
302 Modified Vaccinia Ankara virus (MVA), a DNA virus belonging to the *poxviridae* family, that was
303 engineered to express GFP (MVA-GFP). Flow cytometry analysis using an antibody against the viral
304 protein G revealed that VSV was highly dependent on APOL1 and APOL3 expression for efficient
305 replication in IFNα2-treated HMC3 cells (Fig. 3I). Optimal replication of MeV-GFP in stimulated
306 HMC3 cells also required APOL1 and APOL3 expression (Fig. 3I). APOL1 proviral activity was also
307 observed in unstimulated cells (Fig. 3I). By contrast, MVA-GFP replication was not affected by reduced
308 expression of either APOL1 or APOL3 (Fig. 3I).

309 Together, these experiments suggest that APOL1 and APOL3 could favor a replication process
310 shared by ZIKV, DENV-2, WNV, VSV and MeV. Unlike APOL1 in HMC3 cells, APOL3 pro-viral
311 activities were dependent on IFN-treatment.

312

313 **APOL1 and APOL3 likely promote viral replication independently of their interaction with**
314 **phosphoinositides**
315 Recent data revealed that APOL1 and APOL3 play a role in lipid metabolism in podocytes and, more
316 specifically, in the regulation of the production of phosphatidylinositol-4-phosphate (PI(4)P), via an
317 indirect interaction with the PI4KB kinase [41]. PI(4)P is involved in Golgi secretory functions by
318 facilitating the recruitment of proteins that promote vesicular transport [42]. PI(4)P is also essential for
319 the establishment of efficient viral replication via the formation of membranes which serve as platforms
320 for the production of viral RNA [43,44]. APOL1 and/or APOL3 could thus impact ZIKV replication via
321 their ability to regulate the production of PI(4)P. To test this hypothesis, we first assessed APOL1 and
322 APOL3 localization in HMC3 cells. In the absence of specific antibodies for APOL1 and APOL3
323 validated for immunofluorescence assays, we investigated the localization of GFP-tagged versions of
324 APOL3 and APOL1 in HMC3 cells, together with markers for the Golgi apparatus (Fig. 4A), early or
325 late endosomes (Fig. S3). APOL1-GFP and GFP-APOL3 localized in closed proximity to the cis-Golgi
326 (Fig. 4A), where PI(4)P and PI4KB localize [45], and not in late nor early endosomes (Fig. S3). In line
327 with this, APOL1-GFP and GFP-APOL3 associated with PI4KB in HMC3 cells (Fig. 4B). Of note,
328 APOL1-GFP was also detected in vesicle-like structures whose identity could not be established (Fig.
329 4A, white arrow). They may represent lipid droplets or fragmented Golgi. The localization of APOL1-
330 GFP and GFP-APOL3 could not be investigated in ZIKV-infected cells since we observed that
331 transfection rendered cells non-permissive to viral infection.
332 We then performed experiments with a well-characterized PI4KB kinase inhibitor that decreases
333 PI(4)P expression [46]. We first analyzed by immunofluorescence the intensity of the PI(4)P signal in
334 cells treated for 24 h with different concentrations of the drug in HCM3 cells. The presence of the PI4KB
335 inhibitor triggered a dose-dependent decrease of the PI(4)P signal (Fig. 4C), suggesting that the drug is
336 efficient in HMC3 cells. We then infected cells with ZIKV in the presence of different concentration of
337 the inhibitor. Since the effect of APOL3 on ZIKV replication is dependent on IFNα2 (Fig. 3), the
338 analysis was also performed in stimulated cells. Coxsackie B3 virus (CVB3), an enterovirus that
339 replicates in a PI(4)P-dependent manner, was used as a positive control since its replication is sensitive
340 to the drug [47]. As negative controls, we used cells infected with WNV, whose replication is not
341 affected by the PI4KB inhibitor [48]. As previously shown in HeLa cells [47], a dose-dependent
342 reduction of the number of cells positive for the CVB3 viral protein 1 (VP1) was triggered by the
343 inhibitor treatment (Fig. 4D). As shown previously in monkey cells [48], WNV replication was
344 unaffected by the PI4KB inhibitor in HCM3 cells (Fig. 4D). ZIKV protein production was not sensitive
345 to the treatment with the PI4KB kinase inhibitor, independently of the presence of IFNα2 (Fig. 4D).
346 These experiments suggest that the pro-viral activities of APOL1 and APOL3 are not related to their
347 interaction with PI4KB or PI(4)P in microglial cells.
348
349 **MTA2 restricts ZIKV replication in IFNα2-stimulated human cells.**

350 MTA2 was identified in our screen as a gene with potent anti-ZIKV activities (Fig. 1). MTA2 shows
351 a very broad expression pattern and is strongly expressed in many tissues. It belongs to the NuRD
352 complex, which establishes transcriptional modulation of a number of target genes in vertebrates,
353 invertebrates and fungi [27]. Since its function has, so far, not been linked to viral infection, we decided
354 to investigate its potential antiviral activities further. To ensure that the MTA2-mediated inhibition of
355 viral replication was not restricted to HMC3 cells, experiments were also performed in Huh-7 hepatoma
356 cells, which are physiologically relevant for flavivirus infection and are thus extensively used in
357 *Flaviviridae* research. siRNAs targeting IFNAR1 were used as positive controls in these experiments.
358 siRNA-silencing reduced the levels of MTA2 and IFNAR1 mRNAs by at least 80%, when compared to
359 cells expressing scrambled control siRNAs, independently of the stimulation or infection status of
360 HMC3 and Huh-7 cells (Fig. 5A-D). MTA2 was included in our gene list because its expression
361 clustered with MX1 in T cells (Cerboni et al. in preparation). However, MTA2 mRNA abundance, as
362 measured by RT-qPCR analysis, remained unchanged upon IFNα2 treatment in both cells types (Fig.
363 5A and 5C), indicating that MTA2 is not an ISG in these cells.
364 Assessment of viral replication by RT-qPCR revealed that cell-associated viral RNA yields were
365 significantly higher in IFN-treated HMC3 cells silenced for MTA2 expression, as compared to controls
366 cells (Fig. 5E). This is in line with previous results (Fig. 1E). Cytometry analysis using anti-E antibodies
367 confirmed that MTA2 anti-ZIKV activities were dependent on the presence of IFN in HCM3 cells (Fig.
368 5F). Since MTA2 is not an ISG in HMC3 cells (Fig. 5A), these results suggest that MTA2 may require
369 an active IFN signaling to exert its anti-ZIKV activities in these cells. As in HMC3 cells, reduced
370 expression of MTA2 triggered a significant increase of intracellular viral RNA production in stimulated
371 Huh-7 cells (Fig. 5G). Reducing MTA2 expression had a more pronounced effect on the percentage of
372 infected cells that reducing IFNAR1 expression in stimulated Huh-7 cells (Fig. 5H). Albeit to a lesser
373 extent than in stimulated cells, MTA2 anti-ZIKV activity was also observed in non-stimulated Huh-7
374 cells by flow cytometry and RT-qPCR analysis (Fig. 5G and H).
375 The effect of MTA2 on viral protein production was further assessed by Western blot analysis using
376 anti-E and anti-NS5 antibodies in stimulated and unstimulated HMC3 and Huh-7 cells. These
377 experiments validated further the efficacy of the siRNAs against MTA2 in both cell lines (Fig. 5I and
378 5J). Expression of the viral proteins NS5 and E were increased in stimulated HMC3 and Huh-7 cells
379 expressing reduced levels of MTA2 or IFNAR1, as compared to control cells (Fig. 5I and 5J). In
380 agreement with the flow cytometry analysis (Fig. 5H), MTA2 anti-ZIKV activity was less dependent of
381 IFN-treatment in Huh-7 cells than in HMC3 cells (Fig. 5I and 5J). As observed in flow cytometry
382 analysis (Fig. 5H), MTA2 effect on viral protein production was more potent than the one of IFNAR1
383 in stimulated Huh-7 cells (Fig. 5J).
384 These results represent the first evidence of the ability of MTA2 to restrict the replication of any
385 virus.
386

387 **MTA2 restricts YFV and WNV replication in IFNα2-stimulated Huh-7 cells.**

388 We tested whether MTA2 was active against WNV and YFV in Huh-7 cells, which are permissive
389 to these 2 flaviviruses. As in previous experiments, higher MOIs were used in the presence of IFNα2.
390 Cytometry analysis revealed that MTA2 silencing significantly enhanced the replication of these 2
391 flaviviruses in an-IFN dependent manner (Fig. 6A and 6B), indicating that MTA2 antiviral activity is
392 broader that ZIKV. We then tested the effect of MTA2 silencing on the replication of VSV and MeV in
393 Huh-7 cells. Reduced expression of MTA2 decreased the number of cells infected with VSV and MeV
394 (Fig. 6C and 6D), independently of the IFN stimulation. This is consistent with the pro-HCV activity of
395 MTA2, as measured by titration in stimulated Huh-7.5 cells (Fig. 2B). MTA2 may thus possesses a
396 flavivirus genus-specific antiviral function.

397

398 **Discussion**

399 Several gain-of-fonction screens have been performed to identify ISGs that modulate flavivirus
400 infection. Pionner screens tested the activities of relatively small amounts of ISGs by overexpression
401 [49,50]. The first comprehensive overexpression screen in which more than 380 ISGs were evaluated
402 for antiviral activity against six viruses, including the *Flaviviridae* HCV, WNV and YFV, was published
403 in 2011 by Schoggins and collaborators [21]. To avoid potential physiological irrelevance induced by
404 gene overexpression, we opted for a silencing approach to identify genes that modulate ZIKV replication
405 in an IFN-induced state. We used a siRNA library which was designed in the context of an HIV project.
406 A limitation of our library is that targeted genes were selected based on a transcriptomic analysis of
407 primary T cells stimulated by contacts with activated monocytes (Cerboni et al. in preparation), and not
408 on ZIKV-target cells. Nevertheless, it contains a high fraction of core ISGs that overlaps with previous
409 screens [21,22]. Furthermore, most arrayed screens designed to identify cellular factors that modulate
410 ZIKV replication, including ours, monitored viral replication after a single round of infection, often by
411 assessing viral protein expression. Therefore, only genes that inhibit early stages of viral replication, up
412 to protein production, can be identified. Quantifying viral titers in supernatants collected from individual
413 wells of the first round of screening should identify genes that affect late stages of viral replication, such
414 as viral assembly, maturation and release, as well as viral infectivity. Alternatively, viral replication
415 could be monitored after several rounds of infection. Nevertheless, despite these two main limitations,
416 our screening strategy identified 21 genes affecting the number of cells positive for the viral protein E
417 in IFN-treated microglial cells.

418 Some hits were previously described as ISGs able to modulate ZIKV replication, such as IFITM3
419 [19,20] and LY6E [24], thus validating our screening approach. Despite being in our gene list, Viperin,
420 IFI6, PARP-12 and C19orf66, which are known to affect ZIKV replication in human cells [51–55], were
421 not identified as viral modulators by our strategy. They may have a weaker influence on viral replication
422 in HMC3 cells than in the cells in which their role was previously established [51–55]. In line with this

423 hypothesis, Viperin restricts the replication of several neurotropic flaviviruses in a cell type-dependent
424 manner [56]. One can also envisage that the expression levels of Viperin, IFI6, PARP-12 and C19orf66
425 are low in HMC3 cells, even when stimulated by IFNα2, and therefore are poorly, if at all downregulated
426 by specific siRNAs.

427 We validated the role of 5 hits as genes contributing to an optimal ZIKV replication in stimulated
428 HMC3 cells using RT-qPCR and flow cytometry analysis: LY6E, USP18, ISG15, APOL3 and NAPA.
429 The identification of LY6E as a gene enhancing ZIKV replication was expected, since it was previously
430 shown to promote the internalization of flaviviruses in U2OS human osteosarcoma cells [24]. Since
431 ISG15 and USP18 negatively regulate IFN signaling pathway [57,58], they are expected to act as broad
432 pro-viral ISGs. NAPA interacts with SNARE protein complexes to trigger their disassembly [59].
433 SNARE proteins belong to a superfamily of membrane fusion proteins that localize at the plasma
434 membrane, the Golgi apparatus and on different endocytic vesicles. They regulate the traffic of these
435 vesicles between the plasma membrane and the Golgi [60]. Several viruses, including influenza A virus
436 and VSV, hijack SNARE proteins to enter host cells [61]. SNARE complexes may thus contribute to
437 NAPA pro-viral activities. We validated the anti-viral functions of 4 screen hits in stimulated HMC3
438 cells infected with ZIKV: IRF9, IFITM3, MTA2 and GPD2. Identification of IRF9, which plays a key
439 role in ISG expression [25], and IFITM3, which restricts early stages of ZIKV infection [19,20],
440 validates our screening strategy. GPD2 is a mitochondrial protein involves in the metabolism of
441 glycerol. No link between GPD2 and viral infections has been established yet. However, it regulates
442 inflammatory response in macrophages [62]. Further experiments will be required to confirm that NAPA
443 and GPD2 have the ability to modulate ZIKV replication in stimulated human cells.

444 Experiments performed on cells infected with HCV or SARS-CoV-2 contributed to delineate the
445 spectrum of action of a selection of the screen hits. Our data illustrate once again that some ISGs have
446 virus-specific antiviral activities [63]. For instance, we found that ZIKV, but not the related HCV, was
447 sensitive to IFITM3 expression, confirming (HCV) and extending (ZIKV) recently reported data
448 [20,64]. Our data also confirm that some ISGs exert opposite effect on different viruses. For instance,
449 as described previously, LYE6 promotes the replication of ZIKV [24] but restricts that of SARS-CoV-
450 2 [35]. Viruses have developed numerous innovative strategies to evade ISG-mediated restriction
451 [65,66]. Hijacking individual ISG for promoting their replication is one of them. This hypothesis may
452 explain why, to our surprise, our screen recovered more pro-viral genes that antiviral ones.

453 Our results identified APOL3 and APOL1 as ISGs required for optimal ZIKV replication in HMC3
454 cells. The proviral activity of APOL1 was less dependent on IFN that the one of APOL3, which suggest
455 that both proteins act via different mechanisms. Reduced expression of APOL1 and APOL3 also
456 restricted the replication of WNV and DENV in stimulated HMC3 cells. In line with these findings,
457 over-expression of APOL1 was previously reported to increase YFV replication in Huh-7 cells [21].
458 VSV replication was highly reduced in the absence of one of these 2 genes. APOL1 has been reported
459 to act as an antiviral ISG in the context of infection with alphaviruses (Sindbis virus and Venezuelan

460 equine encephalitis virus) and human parainfluenza virus [21,67]. Its over-expression also inhibits HIV-
461 1 infection in monocytes [68]. Thus, APOL1 and APOL3 seem to behave like pro- or anti-viral ISG
462 depending on the virus, or have no obvious role (HCV). In line with our data on flaviviruses, a recent
463 report found that overexpression of APOL1 promoted infection with ZIKV and DENV-2, confirming a
464 proviral role for this factor [69]. However in this study, an increase of ZIKV, DENV-2 and HCV
465 replication was also reported in Huh-7.5 cells expressing siRNAs targeting APOL1 and APOL3 in the
466 absence of IFN treatment [69], yielding conflicting data that will deserve further investigation.
467 From our data, we formulated the hypothesis that APOL1 and APOL3 pro-viral activities could be
468 linked to their ability to bind to anionic phospholipids, including several phosphoinositides, in particular
469 PI(4)P [41]. Both APOL1 and APOL3 were detected in PI(4)P-containing liposomes [41]. Moreover,
470 reduced expression of APOL3 resulted in reduction of PI(4)P levels in podocytes [41]. PI(4)P plays a
471 pivotal role in the Golgi secretory functions by facilitating recruitment of proteins that promote vesicular
472 transport [42]. Our immunofluorescence data revealed that GFP-tagged version of APOL1 and APOL3
473 localize mainly in the Golgi, where PI(4)P localizes [42]. Numerous RNA viruses, including various
474 *Picornaviridae,* HCV, coronaviruses and parainfluenza type 3, rely on PI(4)P to build membranous
475 replication platform, where viral replication and assembly take place [70]. Flaviviruses are no exception
476 and also trigger intracellular membrane remodelling for the building of membranous replication
477 platforms [71]. Experiments conducted with a well-characterized PI4KB kinase inhibitor excluded the
478 possibility that APOL1 and APOL3 pro-viral effects depend on PI(4)P and its synthetizing protein,
479 PI4KB. In line with these results, PI(4)P are not important for the replication of WNV and the related
480 Usutu virus [48]. Other avenues should be thus explored to understand how APOL1 and APOL3
481 modulate the replication of several RNA viruses. Since APOL1 and APOL3 impact the replication of
482 unrelated viruses, they may be negative regulators of IFN signalling pathway, by, for instance,
483 contributing to the proper routing of members of the JAK/STAT pathway.
484 Our data revealed that MTA2 possesses potent antiviral function in the context of ZIKV, WNV and
485 YFV in stimulated cells, whereas its exhibited a proviral role for HCV, VSV and MeV. Reducing MTA2
486 expression in the presence of IFNα2 enhanced flaviviral replication to a level comparable to the
487 inhibition of IFNAR1. Despite being part of our gene list, MTA2 is not induced by IFN in HMC3 Huh-7
488 cells but its antiviral activity was dependent on IFN in these cells. MTA2 may thus interact with an ISG
489 to act on viral replication. MTA2 is a component of the NuRD complex, an unusual complex which
490 exhibits ATP-dependent chromatin remodeling activity in addition to histone deacetylase activity [27].
491 The complex establishes transcriptional modulation of a number of target genes in vertebrates,
492 invertebrates and fungi [27]. MTA2 related activities have not, so far, been linked to innate immunity
493 in virus-infected cells. However, a link between the NuRD complex and STAT1-mediated IFN response
494 was established in the context of infection with the protozoan parasite *Toxoplasma gondii* [72]. A
495 *Toxoplasma* protein, named TgIST, translocates to the host cell nucleus where it recruits the complex
496 NuRD to STAT1-dependent promoters, resulting in altered chromatin and blocked STAT1-mediated

497 transcription [72]. Moreover, HDAC1, which is also a member of the NuRD complex, associates with
498 both STAT1 and STAT2 in human cells [73]. Furthermore, specific reduction of HDAC1 expression
499 inhibits IFNβ-induced transcription whereas HDAC1 overexpression enhances IFNβ-induced
500 transcription [73]. Finally, HDAC inhibitors block the formation of ISGF3 and this was associated with
501 impairment of STAT2 nuclear accumulation in mouse L929 cells [74]. These findings indicate a
502 fundamental role for deacetylase activity and HDAC1 in transcriptional control in response to IFN. One
503 could thus envisage that MTA2, within the NuRD complex, also interacts with STAT1 in cells
504 stimulated with IFN and favors its action locally. This interaction could restrict flavivirus infection,
505 possibly *via* enhancing the expression of a subset of flavivirus-specific ISGs.
506 Our work identified previously unrecognized genes that modulate the replication of RNA viruses in
507 an IFN-dependent way. Future studies combining transcriptomic analysis of IFN-treated cells and high
508 throughput loss-of-function screens will help define the interferome of cell types relevant for viral
509 infection. Such studies are primordial to continue investigating the complexity the IFN-mediated
510 antiviral program.
511
512
513 **Materials and Methods**
514
515 **Cells**
516 Human microglial cells (HMC3) were purchased from the American Type Culture Collection (ATCC,
517 CRL-3304). They were maintained in Dulbecco's modified Eagle's medium (DMEM) containing
518 GlutaMAX I and sodium pyruvate (Gibco), supplemented with 10% fetal bovine serum (FBS) and 1%
519 penicillin-streptomycin (P/S) (final concentration of 100 units/mL and 100 µg/mL, respectively)
520 (Sigma) and non-essential amino acids (GibcoTM NEAA 100X MEM, Life Technologies). Podocytes
521 were described previously [75]. They were grown at 33°C in Roswell Park Memorial Institute medium
522 (RPMI) containing GlutaMAX I (Gibco) and supplemented with 10% FBS and P/S. Before any
523 experiments, cells were differentiated during 7 days at 37°C. Human hepatocellular carcinoma Huh-7
524 cells [76], which were kindly given by Cinzia Traboni (IRBM, Pomezia, Italy), were maintained in
525 DMEM supplemented with 10% FBS and 1% P/S. Huh-7.5 cells (Apath, LLC), a subclone of Huh-7
526 cells [76] were cultured in DMEM supplemented with non-essential amino acids, 1mM sodium
527 pyruvate, 10% FBS and P/S. Vero NK cells, which are African green monkey kidney epithelial cells,
528 were purchased from ATCC and used for viral titration assays. They were maintained in DMEM
529 containing GlutaMAX I and sodium pyruvate (Gibco), supplemented with 10% FBS and P/S. *Aedes*
530 *albopictus* C6-36 cells were maintained in Leibovitz's L-15 medium containing 10% FBS, 1% P/S, 1%
531 Non-Essential Amino Acids Solution (Gibco) and 2% Tryptose Phosphate Browth (Gibco). Human lung
532 epithelial A549 cells were modified to stably express hACE2 using the pLenti6-hACE2 lentiviral

533 transduction, as described previously [77]. Cell cultures were verified to be mycoplasma free with the
534 MycoAlertTM Mycoplasma Detection Kit (Lonza).
535
536 **Virus stocks, titration and infection**
537 The Zika strain PF13 (kindly provided by V. M. Cao-Lormeau and D. Musso, Institut Louis Malardé,
538 Tahiti Island, French Polynesia) was isolated from a viremic patient in French Polynesia in 2013. Stocks
539 were produced on C6-36 cells. The Dengue 2 virus (DENV-2) strain Malaysia SB8553 was obtained
540 from the Centro de Ingeniería Genética y Biotecnología (CIGB), Cuba. The YFV Asibi strain and the
541 WNV Israeli strain IS-98-STI were provided by the Biological resource Center of the Institut Pasteur.
542 Stocks of DENV-2, YFV and WNV were produced on Vero NK cells. Viruses were concentrated by
543 polyethylene glycol 6000 precipitation and purified by centrifugation in a discontinued gradient of
544 sucrose. Flaviviruses were titrated on Vero NK cells by plaque assay as previously described [78] and
545 titers were expressed in plaque-forming units (PFU)/ml. The Measles Schwarz strain expressing GFP
546 (MeV-GFP) was described previously [40]. VSV Indiana and the CVB3 Nancy strain were kindly
547 provided by N. Escriou (Institut Pasteur) and M. Bessaud, respectively (Institut Pasteur). Modified
548 Vaccinia Ankara virus (MVA) expressing eGFP (MVA-GFP) was kindly provided by the ANRS via O.
549 Schwartz (Institut Pasteur). It was manufactured by Transgene (Illkirch-Graffenstaden, France).
550 The fluorescent marker, eGFP, is expressed under the control of the early promotor p11K7.5 and viral
551 preparations were purified by tangential flow filtration. HMC3 cells were infected at the following
552 MOIs: a MOI of 10 with DENV-2, 0,5 with WNV, 0,005 with VSV, 1 with MeV-GFP and 0,05 with
553 MVA-GFP. IFN-treated HMC3 cells were infected at a MOI of 20 with DENV-2, 5 with WNV, 0,01
554 with VSV, 2 with MeV-GFP and 0,25 with MVA-GFP. Huh-7 were infected at a MOI of 1 with YFV
555 and 0,25 with WNV. IFN-treated Huh-7 cells were infected at a MOI of 10 with YFV and WNV. Highly
556 cell culture-adapted HCV Jad strain was obtained following transfection of Huh-7.5 cells with *in vitro*
557 transcribed genome-length RNA as described previously [79–81]. Large volumes of HCV stocks were
558 prepared following infection at a MOI of 0.01 50% tissue culture infectious doses 50 (TCID50) per cell
559 with supernatants collected post-RNA transfection [82]. HCV infectious titers were determined by
560 TCID50 assays in Huh-7.5 cells as described previously [79]. IFN-treated Huh-7.5 cells were infected
561 at MOI of 3 TCID50/cell with HCV. The SARS-CoV-2 strain BetaCoV/France/IDF0372/2020
562 (historical) was supplied by the French National Reference Centre for Respiratory Viruses hosted by
563 Institut Pasteur (Paris, France) and headed by Pr. S. van der Werf. The human samples from which the
564 strain was isolated were provided by Dr. X. Lescure and Pr. Y. Yazdanpanah from the Bichat Hospital,
565 Paris, France and Dr. Vincent Foissaud, HIA Percy, Clamart, France, respectively. A549-ACE2 cells
566 were infected with SARS-CoV-2 at a MOI of 2.
567
568 **High throughput Screen**

569 Five hundreds HMC3 cells were seeded in 384-well microplates in the morning of day 1 using a
570 MultiDrop combi liquid dispenser (Thermo Fisher Scientific), in 40 µL of cell culture media. Cells were
571 allowed to adhere for 4 hours (+/-1h) before transfection with individual siRNAs (10nM) diluted in a
572 mix of OptiMEM (Life Technologies) and 0.05µL of Interferin reagent (Polyplus Transfection). siRNAs
573 were transfected using an Evo 150 with MCA384 (Tecan). The library contained 1158 siRNA targeting
574 386 genes. siRNA targeting KIF11 was used to assess the transfection efficiency. On day 2, cells were
575 treated with 1000U/ml of IFNα2a. Interferon was diluted into cell culture media and 10µL of the mix
576 was robotically transferred to each well (except non-treated controls). 24 hours after IFN treatment, cell
577 media was removed from siRNA-transfected plates and 40µL of the ZIKV PF13 strain, diluted to a final
578 concentration of 7,500 particles/well, was added to the plates with the MCA384 head (Tecan). ZIKV
579 titer was $6.5.10^8$ PFU/ml. Cells were then incubated 24 hours prior to fixation. Cells were fixed with 4%
580 of formaldehyde (Sigma-Aldrich) for 20 min, plates were then washed once with PBS and quenched
581 with NH4Cl (50mM) solution. Cells were then blocked with 1% BSA solution and permeabilized with
582 0.5% Triton X-100. Cells were next incubated for 60 min with mouse primary antibody anti-4G2 (1:500)
583 which reacts with flavivirus E proteins. Cells were then washed twice in PBS solution and incubated
584 with Alexa Fluor 488-coupled secondary antibodies (ThermoFisher Scientific). Nuclei were stained with
585 0.2 µg/ml Hoechst (Sigma). Images were acquired with an INCell2200 automated wide-field system
586 (GE Healthcare,) using a Nikon 10X/0.45, Plan Apo, CFI/60. Three fields per well were analyzed using
587 the INCell Analyzer 3.7 Workstation software. Two independent screens were performed. The mean
588 cell count and the percentages of infected cells were extracted from quantification.
589
590 **Data analysis and hit calling**
591 In the first analysis, data were processed using a software developed internally at the Biophenics
592 platform. For hit identification, the robust Z-score method was used under the assumption that most
593 siRNAs are inactive against ZIKV and can serve as controls [83,84]. Raw values were log-transformed
594 for cell count only to make the data more symmetric and close to normal distribution. In order to correct
595 for plate positional effects, median polishing [84] was applied to each analyzed feature. It iteratively
596 subtracts row, column and well median, computed from all plates within one screen. Hits for each
597 compound were identified as follows: sample median and median absolute deviation (MAD) were
598 calculated from the population of screening data points (named as sample) and used to compute Robust
599 Z-scores (RZ-scores) according to a formula, in which the reference population corresponds to the
600 siRNA-treated wells, and MAD is defined as the median of the absolute deviation from the median of
601 the corresponding wells:
602

$$rZ\text{-}Score = \frac{x - med(pop\ réf)}{1.4826\ x\, med(|pop\ réf - med(pop\ réf)|)}$$

603

604 A gene was identified as a 'hit', if the RZ-score was < -2 or > 2 pointing in the same direction for 2
605 siRNAs targeting the same gene in both screens. Final values in the hit table correspond to the RZ-score
606 of the second strongest siRNA. In the second analysis, data were process using an homemade script and
607 CellProfiler [85]. Nucleus and viral assembly sites detected by the E signal were counted. As in the first
608 analysis, rZ-Score and percentages of infected cells were quantified. Considering that each gene was
609 targeted by three individual siRNA, genes were clusterized as hits, if at least two over three of their
610 robust Z score absolute value were superior to 2. Genes were defined as hits when they were identified
611 in at least one of the analysis.
612
613 **Antibodies, plasmids and reagents**
614 The following primary antibodies were used in the study: anti-E MAb 4G2 hybridoma cells, anti-NS5-
615 ZIKV [86], anti-VSV-G (IE9F9, Kerafast), anti-CVB3 VP1 (M7064, Agilent), anti-SARS-CoV-2 S
616 protein mAb10 (1 µg/ml, a kind gift from H. Mouquet, Institut Pasteur, Paris, France), APOL1
617 (HPA018885, Sigma), MTA2 (8106, abcam), GM130 (12480, cell signaling), PI(4)P (Z-P004), PI(4)KB
618 (06-578, Milipore) and anti-actin (A5316, Sigma). Secondary antibodies were as followed: anti-mouse
619 Alexa 488 (A11001, Life Technologies), anti-mouse Alexa 680 (A21058, Life Technologies) and anti-
620 rabbit DyLight 800 (SA5-35571, TermoScientific). The PI4KB inhibitor (1881233-39-1,
621 MedChemExpress) and IFNα2a (Sigma-Aldrich, SRE0013) were used at the indicated concentration.
622 GFP-APOL3 et APOL3-GFP were subcloned into pcDNA.3.1 from templates previously described
623 [41].
624
625 **siRNA transfection**
626 HMC3 cells were transfected using INTERFERin transfection reagent (Polyplus Transfection). Huh-7
627 cells, Huh-7.5 cells and podocytes were transfected with siRNAs at 10 nM final concentration using
628 Lipofectamine RNAiMax (Life Technologies). All siRNAs were obtained from Dharmacon
629 (siGENOME-SMARTpool).
630
631 **RNA extraction and RT-qPCR assays**
632 Total RNAs were extracted from cell lysates using the NucleoSpin RNA II Kit (Macherey-Nagel)
633 following the manufacturer's protocol and were eluted in nuclease-free water. First-strand
634 complementary DNA synthesis was performed with the RevertAid H Minus M-MuLV Reverse
635 Transcriptase (Thermo Fisher Scientific). Quantitative real-time PCR was performed on a real-time PCR
636 system (QuantStudio 6 Flex, Applied Biosystems) with SYBR Green PCR Master Mix (Life
637 Technologies). Data were analyzed with the ΔΔCT method, with all samples normalized to GAPDH.
638 All experiments were performed in technical triplicate. Viral genome equivalents concentrations
639 (GE/ml) were determined by extrapolation from a standard curve generated from serial dilutions of the
640 plasmid encoding the full-length genome of the Zika strain MR766 [87] or plasmids encoding a

641 fragment of the RNA-dependent RNA polymerase (RdRp)-IP4 of SARS-CoV-2. HCV RNA was
642 quantified by one-step reverse transcription-quantitative PCR using 50 ng of total intracellular RNA and
643 TaqMan® Fast Virus 1-Step Master Mix (Applied Biosystems) with primers and probe targeting the
644 HCV 5′ nontranslated region as described previously [82]. Viral RNA levels were normalized with
645 respect to 18S RNA levels quantified in parallel using TaqMan ribosomal RNA control reagents
646 (Applied Biosystems). The products were analysed on a 7500 Fast Real-Time PCR system (Applied
647 Biosystems). Serial dilutions of a genome-length *in vitro* transcribed HCV RNA served to establish
648 standard curves and calculate HCV GE/µg total RNA concentrations. Primers and probe used for RT-
649 qPCR analysis are given in Table S2.
650
651 **Western blot analysis**
652 Cells were collected in RIPA buffer (Sigma) containing protease inhibitors (Roche Applied Science).
653 Cell lysates were normalized for protein content with Pierce 660nm Protein Assay (Thermo Scientific),
654 boiled in NuPAGE LDS sample buffer (Thermo Fisher Scientific) in non-reducing conditions. Samples
655 were separated by SDS-PAGE (NuPAGE 4–12% Bis-Tris Gel, Life Technologies) with MOPS running
656 buffer. Separated proteins were transferred to a nitrocellulose membrane (Bio-Rad). After blocking with
657 PBS-Tween-20 0.1% (PBST) containing 5% milk for 1 h at RT, the membrane was incubated overnight
658 at 4°C with primary antibodies diluted in blocking buffer. Finally, the membranes were incubated for 1
659 h at RT with secondary antibodies diluted in blocking buffer, washed, and scanned using an Odyssey
660 CLx infrared imaging system (LI-COR Bioscience).
661
662 **Flow cytometry**
663 Infected cells were fixed with cytofix/cytoperm kit (BD Pharmingen) and stained using the indicated
664 primary and secondary antibodies. Non-infected, antibody-stained samples served as controls for signal
665 background. Data were acquired using Attune NxT Acoustic Focusing Cytometer (Life Technologies)
666 and analyzed using FlowJo software.
667
668 **Immunofluorescence assay**
669 Cells were fixed with PFA 4% (Sigma) during 20min. Cells were permeabilized with PBS Triton X-100
670 (0.5%) for 15min at RT. After washing with PBS, they were incubated for 30 min with PBS + 0.05%
671 Tween 20 + 5% BSA. The slides were then incubated overnight at 4°C with primary antibodies diluted
672 in PBS. After washing with PBS, they were incubated for 1 h with secondary antibodies and washed
673 with PBS. Nuclei were stained using PBS/NucBlue (Life Technologies, R37606). The mounting
674 medium used is the Prolong gold (Life Technologies, P36930). All preparations were observed with a
675 confocal microscope (ZEISS LSM 700 inverted) and images were acquired with the ZEN software.
676
677 **Statistical analysis.**

Data are presented as means ± SD and were analyzed using GraphPad Prism 7. Statistical analysis of percentage values or fold enrichment values were performed on logit or log-transformed values, respectively. Statistical analysis was performed with two tailed paired t-test or by one- or two-way analysis of variance (ANOVA) with Dunnet's multiple comparisons test. Each experiment was performed at least twice, unless otherwise stated. Statistically significant differences are indicated as follows: *: $p < 0.05$, **: $p < 0.01$ and ***: $p < 0.001$; ns, not significant.

Acknowledgments

We thank Dr. M.A. Saleem (University of Bristol, UK) for generously providing the podocytes (via E. Pays, Université Libre de Bruxelles, Belgium); C.M. Rice (Rockefeller University, New York, USA) for Huh-7.5 cells; Cinzia Traboni (IRBM, Pomezia, Italy) for Huh-7 cells; M. Bessaud (Institut Pasteur) for the CVB3 Nancy strain; N. Escriou (Institut Pasteur) for the VSV Indiana strain and anti-VSV-G antibodies; V. M. Cao-Lormeau and D. Musso (Institut Louis Malardé, Tahiti Island, French Polynesia) for the ZIKV-PF13 strain; L. Hermida and G. Enrique Guillen Nieto from the Centro de Ingeniería Genética y Biotecnología (CIGB), Cuba, for the DENV-2 strain Malaysia SB8553; T. Wakita (NIID, Tokyo, Japan) for pJFH1 HCV cDNA; R. Bartenschlager (University of Heidelberg, Germany) for pJFH1-2EI3-adapt cDNA; the French National Reference Centre for Respiratory Viruses hosted by Institut Pasteur (France) and headed by S. van der Werf for providing the historical SARS-CoV-2 viral strains; A. Merits (University of Tartu, Estonia) for anti-ZIKV NS5 antibodies; P. Desprès (Université de la Réunion, PIMIT) for 4G2 hybridoma cells; H. Mouquet (Institut Pasteur) for anti-SARS-CoV-2 S antibodies; M. Evans (Icahn School of Medicine at Mount Sinai, New York, USA) for the plasmid encoding the full-length Zika MR766 genome; F. Porrot and O. Schwartz (Institut Pasteur) for producing and sharing the MVA-GFP, C. Combredet (Institut Pasteur) for producing MeV-GFP; as well as E. Pays and S. Uzureau (Université Libre de Bruxelles, Belgium) for APOL1 and APOL3 plasmids and for stimulating APOL-focused discussions. We are grateful to the members of our laboratories for helpful discussions and technical advice. Finally, we thank Emeline Perthame (Bioinformatics and Biostatistics HUB, Institut Pasteur) for her help in statistical analysis.

Declaration of interests. The authors declare no competing interests.

References

1. Woolhouse M, Scott F, Hudson Z, Howey R, Chase-Topping M. Human viruses: discovery and emergence. Philos Trans R Soc Lond B Biol Sci. 2012;367: 2864–71. doi:10.1098/rstb.2011.0354
2. Streicher F, Jouvenet N. Stimulation of Innate Immunity by Host and Viral RNAs. Trends in Immunology. 2019;40: 1134–1148. doi:10.1016/j.it.2019.10.009

716 3. Schoggins JW. Recent advances in antiviral interferon-stimulated gene biology.
717 F1000Res. 2018;7. doi:10.12688/f1000research.12450.1
718 4. Rusinova I, Forster S, Yu S, Kannan A, Masse M, Cumming H, et al. Interferome
719 v2.0: an updated database of annotated interferon-regulated genes. Nucleic Acids Res.
720 2013;41: D1040-6. doi:10.1093/nar/gks1215
721 5. Touzot M, Grandclaudon M, Cappuccio A, Satoh T, Martinez-Cingolani C, Servant N,
722 et al. Combinatorial flexibility of cytokine function during human T helper cell
723 differentiation. Nat Commun. 2014;5: 3987. doi:10.1038/ncomms4987
724 6. Mostafavi S, Yoshida H, Moodley D, LeBoité H, Rothamel K, Raj T, et al. Parsing the
725 interferon transcriptional network and its disease associations. Cell. 2016;164: 564–578.
726 doi:10.1016/j.cell.2015.12.032
727 7. Schneider WM, Chevillotte MD, Rice CM. Interferon-Stimulated Genes: A Complex
728 Web of Host Defenses. Annu Rev Immunol. 2014;32: 513–545. doi:10.1146/annurev-
729 immunol-032713-120231
730 8. Pierson TC, Diamond MS. The continued threat of emerging flaviviruses. Nat
731 Microbiol. 2020. doi:10.1038/s41564-020-0714-0
732 9. Ashraf U, Ye J, Ruan X, Wan S, Zhu B, Cao S. Usutu virus: an emerging flavivirus in
733 Europe. Viruses. 2015;7: 219–38. doi:10.3390/v7010219
734 10. Pierson TC, Diamond MS. The emergence of Zika virus and its new clinical
735 syndromes. Nature. 2018;560: 573–581. doi:10.1038/s41586-018-0446-y
736 11. Matusali G, Houzet L, Satie A-P, Mahé D, Aubry F, Couderc T, et al. Zika virus
737 infects human testicular tissue and germ cells. J Clin Invest. 2018;128: 4697–4710.
738 doi:10.1172/JCI121735
739 12. Rossi SL, Tesh RB, Azar SR, Muruato AE, Hanley KA, Auguste AJ, et al.
740 Characterization of a Novel Murine Model to Study Zika Virus. Am J Trop Med Hyg.
741 2016;94: 1362–9. doi:10.4269/ajtmh.16-0111
742 13. Lazear HM, Govero J, Smith AM, Platt DJ, Fernandez E, Miner JJ, et al. A Mouse
743 Model of Zika Virus Pathogenesis. Cell Host Microbe. 2016;19: 720–30.
744 doi:10.1016/j.chom.2016.03.010
745 14. Tripathi S, Balasubramaniam VR, Brown JA, Mena I, Grant A, Bardina SV, et al. A
746 novel Zika virus mouse model reveals strain specific differences in virus pathogenesis and
747 host inflammatory immune responses. PLoS Pathog. 2017;13: e1006258.
748 doi:10.1371/journal.ppat.1006258
749 15. Xia H, Luo H, Shan C, Muruato AE, Nunes BTD, Medeiros DBA, et al. An
750 evolutionary NS1 mutation enhances Zika virus evasion of host interferon induction. Nat
751 Commun. 2018;9: 414. doi:10.1038/s41467-017-02816-2
752 16. Meertens L, Labeau A, Dejarnac O, Cipriani S, Sinigaglia L, Bonnet-Madin L, et al.
753 Axl Mediates ZIKA Virus Entry in Human Glial Cells and Modulates Innate Immune
754 Responses. Cell Rep. 2017;18: 324–333. doi:10.1016/j.celrep.2016.12.045
755 17. Xu P, Shan C, Dunn TJ, Xie X, Xia H, Gao J, et al. Role of microglia in the
756 dissemination of Zika virus from mother to fetal brain. PLoS Negl Trop Dis. 2020;14.
757 doi:10.1371/journal.pntd.0008413
758 18. Wang J, Liu J, Zhou R, Ding X, Zhang Q, Zhang C, et al. Zika virus infected primary
759 microglia impairs NPCs proliferation and differentiation. Biochem Biophys Res Commun.
760 2018;497: 619–625. doi:10.1016/j.bbrc.2018.02.118
761 19. Savidis G, Perreira JM, Portmann JM, Meraner P, Guo Z, Green S, et al. The IFITMs
762 Inhibit Zika Virus Replication. Cell Rep. 2016;15: 2323–30. doi:10.1016/j.celrep.2016.05.074
763 20. Monel B, Compton AA, Bruel T, Amraoui S, Burlaud-Gaillard J, Roy N, et al. Zika
764 virus induces massive cytoplasmic vacuolization and paraptosis-like death in infected cells.
765 EMBO J. 2017;36: 1653–1668. doi:10.15252/embj.201695597

766 21. Schoggins JW, Wilson SJ, Panis M, Murphy MY, Jones CT, Bieniasz P, et al. A
767 diverse range of gene products are effectors of the type I interferon antiviral response. Nature.
768 2011;472: 481–5. doi:10.1038/nature09907
769 22. Liu S-Y, Sanchez DJ, Aliyari R, Lu S, Cheng G. Systematic identification of type I
770 and type II interferon-induced antiviral factors. PNAS. 2012;109: 4239–4244.
771 23. Groth-Pedersen L, Aits S, Corcelle-Termeau E, Petersen NHT, Nylandsted J, Jäättelä
772 M. Identification of cytoskeleton-associated proteins essential for lysosomal stability and
773 survival of human cancer cells. PLoS One. 2012;7: e45381.
774 doi:10.1371/journal.pone.0045381
775 24. Hackett BA, Cherry S. Flavivirus internalization is regulated by a size-dependent
776 endocytic pathway. Proc Natl Acad Sci U S A. 2018;115: 4246–4251.
777 doi:10.1073/pnas.1720032115
778 25. Paul A, Tang TH, Ng SK. Interferon Regulatory Factor 9 Structure and Regulation.
779 Front Immunol. 2018;9. doi:10.3389/fimmu.2018.01831
780 26. Smith S, Weston S, Kellam P, Marsh M. IFITM proteins-cellular inhibitors of viral
781 entry. Curr Opin Virol. 2014;4: 71–77. doi:10.1016/j.coviro.2013.11.004
782 27. Lai AY, Wade PA. NuRD: A multi-faceted chromatin remodeling complex in
783 regulating cancer biology. Nat Rev Cancer. 2011;11: 588–596. doi:10.1038/nrc3091
784 28. Blight KJ, McKeating JA, Rice CM. Highly permissive cell lines for subgenomic and
785 genomic hepatitis C virus RNA replication. J Virol. 2002;76: 13001–14.
786 29. Sumpter R, Loo YM, Foy E, Li K, Yoneyama M, Fujita T, et al. Regulating
787 intracellular antiviral defense and permissiveness to hepatitis C virus RNA replication
788 through a cellular RNA helicase, RIG-I. J Virol. 2005;79: 2689–99.
789 doi:10.1128/JVI.79.5.2689-2699.2005
790 30. Mukherjee A, Di Bisceglie AM, Ray RB. Hepatitis C virus-mediated enhancement of
791 microRNA miR-373 impairs the JAK/STAT signaling pathway. J Virol. 2015;89: 3356–65.
792 doi:10.1128/JVI.03085-14
793 31. Li Y, Ma MX, Qin B, Lin L-T, Richardson CD, Feld J, et al. The Ubiquitin-Specific
794 Protease 18 Promotes Hepatitis C Virus Production by Increasing Viral Infectivity. Mediators
795 of Inflammation. 2019;2019: e3124745. doi:10.1155/2019/3124745
796 32. Randall G, Chen L, Panis M, Fischer AK, Lindenbach BD, Sun J, et al. Silencing of
797 USP18 Potentiates the Antiviral Activity of Interferon Against Hepatitis C Virus Infection.
798 Gastroenterology. 2006;131: 1584–1591. doi:10.1053/j.gastro.2006.08.043
799 33. Arnaud N, Dabo S, Akazawa D, Fukasawa M, Shinkai-Ouchi F, Hugon J, et al.
800 Hepatitis C virus reveals a novel early control in acute immune response. PLoS Pathog.
801 2011;7: e1002289. doi:10.1371/journal.ppat.1002289 PPATHOGENS-D-11-00682 [pii]
802 34. Chen L, Sun J, Meng L, Heathcote J, Edwards AM, McGilvray ID. ISG15, a
803 ubiquitin-like interferon-stimulated gene, promotes hepatitis C virus production in vitro:
804 implications for chronic infection and response to treatment. J Gen Virol. 2010;91: 382–388.
805 doi:10.1099/vir.0.015388-0
806 35. Pfaender S, Mar KB, Michailidis E, Kratzel A, Boys IN, V'kovski P, et al. LY6E
807 impairs coronavirus fusion and confers immune control of viral disease. Nature Microbiology.
808 2020;5: 1330–1339. doi:10.1038/s41564-020-0769-y
809 36. Vanhollebeke B, Pays E. The function of apolipoproteins L. Cell Mol Life Sci.
810 2006;63: 1937–1944. doi:10.1007/s00018-006-6091-x
811 37. Monajemi H, Fontijn RD, Pannekoek H, Horrevoets AJG. The apolipoprotein L gene
812 cluster has emerged recently in evolution and is expressed in human vascular tissue.
813 Genomics. 2002;79: 539–546. doi:10.1006/geno.2002.6729
814 38. Malakhova OA, Kim KI, Luo J-K, Zou W, Kumar KGS, Fuchs SY, et al. UBP43 is a
815 novel regulator of interferon signaling independent of its ISG15 isopeptidase activity. EMBO

816 J. 2006;25: 2358–2367. doi:10.1038/sj.emboj.7601149
817 39. Alcendor DJ. Zika Virus Infection of the Human Glomerular Cells: Implications for
818 Viral Reservoirs and Renal Pathogenesis. J Infect Dis. 2017;216: 162–171.
819 doi:10.1093/infdis/jix171
820 40. Combredet C, Labrousse V, Mollet L, Lorin C, Delebecque F, Hurtrel B, et al. A
821 Molecularly Cloned Schwarz Strain of Measles Virus Vaccine Induces Strong Immune
822 Responses in Macaques and Transgenic Mice. Journal of Virology. 2003;77: 11546–11554.
823 doi:10.1128/JVI.77.21.11546-11554.2003
824 41. Uzureau S, Lecordier L, Uzureau P, Hennig D, Graversen JH, Homblé F, et al.
825 APOL1 C-Terminal Variants May Trigger Kidney Disease through Interference with APOL3
826 Control of Actomyosin. Cell Rep. 2020;30: 3821-3836.e13. doi:10.1016/j.celrep.2020.02.064
827 42. Waugh MG. The Great Escape: how phosphatidylinositol 4-kinases and PI4P promote
828 vesicle exit from the Golgi (and drive cancer). Biochem J. 2019;476: 2321–2346.
829 doi:10.1042/BCJ20180622
830 43. Delang L, Paeshuyse J, Neyts J. The role of phosphatidylinositol 4-kinases and
831 phosphatidylinositol 4-phosphate during viral replication. Biochem Pharmacol. 2012;84:
832 1400–1408. doi:10.1016/j.bcp.2012.07.034
833 44. Strating JR, van Kuppeveld FJ. Viral rewiring of cellular lipid metabolism to create
834 membranous replication compartments. Curr Opin Cell Biol. 2017;47: 24–33.
835 doi:10.1016/j.ceb.2017.02.005
836 45. Daboussi L, Costaguta G, Ghukasyan R, Payne GS. Conserved role for Gga proteins
837 in phosphatidylinositol 4-kinase localization to the trans-Golgi network. PNAS. 2017;114:
838 3433–3438.
839 46. Rutaganira FU, Fowler ML, McPhail JA, Gelman MA, Nguyen K, Xiong A, et al.
840 Design and Structural Characterization of Potent and Selective Inhibitors of
841 Phosphatidylinositol 4 Kinase IIIβ. J Med Chem. 2016;59: 1830–1839.
842 doi:10.1021/acs.jmedchem.5b01311
843 47. Hsu N-Y, Ilnytska O, Belov G, Santiana M, Chen Y-H, Takvorian PM, et al. Viral
844 reorganization of the secretory pathway generates distinct organelles for RNA replication.
845 Cell. 2010;141: 799–811. doi:10.1016/j.cell.2010.03.050
846 48. Martín-Acebes MA, Blázquez A-B, Jiménez de Oya N, Escribano-Romero E, Saiz J-
847 C. West Nile virus replication requires fatty acid synthesis but is independent on
848 phosphatidylinositol-4-phosphate lipids. PLoS One. 2011;6: e24970.
849 doi:10.1371/journal.pone.0024970
850 49. Jiang D, Weidner JM, Qing M, Pan XB, Guo H, Xu C, et al. Identification of five
851 interferon-induced cellular proteins that inhibit west nile virus and dengue virus infections. J
852 Virol. 2010;84: 8332–41. doi:10.1128/JVI.02199-09
853 50. Itsui Y, Sakamoto N, Kurosaki M, Kanazawa N, Tanabe Y, Koyama T, et al.
854 Expressional screening of interferon-stimulated genes for antiviral activity against hepatitis C
855 virus replication. J Viral Hepat. 2006;13: 690–700. doi:10.1111/j.1365-2893.2006.00732.x
856 51. Van der Hoek KH, Eyre NS, Shue B, Khantisitthiporn O, Glab-Ampi K, Carr JM, et
857 al. Viperin is an important host restriction factor in control of Zika virus infection. Sci Rep.
858 2017;7: 4475. doi:10.1038/s41598-017-04138-1
859 52. Richardson RB, Ohlson MB, Eitson JL, Kumar A, McDougal MB, Boys IN, et al. A
860 CRISPR screen identifies IFI6 as an ER-resident interferon effector that blocks flavivirus
861 replication. Nat Microbiol. 2018. doi:10.1038/s41564-018-0244-1
862 53. Li L, Zhao H, Liu P, Li C, Quanquin N, Ji X, et al. PARP12 suppresses Zika virus
863 infection through PARP-dependent degradation of NS1 and NS3 viral proteins. Sci Signal.
864 2018;11: eaas9332. doi:10.1126/scisignal.aas9332
865 54. Wu Y, Yang X, Yao Z, Dong X, Zhang D, Hu Y, et al. C19orf66 interrupts Zika virus

866 replication by inducing lysosomal degradation of viral NS3. PLOS Neglected Tropical
867 Diseases. 2020;14: e0008083. doi:10.1371/journal.pntd.0008083
868 55. Vanwalscappel B, Gadea G, Desprès P. A Viperin Mutant Bearing the K358R
869 Substitution Lost its Anti-ZIKA Virus Activity. Int J Mol Sci. 2019;20: E1574.
870 doi:10.3390/ijms20071574
871 56. Lindqvist R, Kurhade C, Gilthorpe JD, Överby AK. Cell-type- and region-specific
872 restriction of neurotropic flavivirus infection by viperin. Journal of Neuroinflammation.
873 2018;15: 80. doi:10.1186/s12974-018-1119-3
874 57. Perng Y-C, Lenschow DJ. ISG15 in antiviral immunity and beyond. Nat Rev
875 Microbiol. 2018;16: 423–439. doi:10.1038/s41579-018-0020-5
876 58. Honke N, Shaabani N, Zhang D-E, Hardt C, Lang KS. Multiple functions of USP18.
877 Cell Death Dis. 2016;7: e2444–e2444. doi:10.1038/cddis.2016.326
878 59. Huang X, Sun S, Wang X, Fan F, Zhou Q, Lu S, et al. Mechanistic insights into the
879 SNARE complex disassembly. Science Advances. 2019;5: eaau8164.
880 doi:10.1126/sciadv.aau8164
881 60. Jahn R, Scheller RH. SNAREs — engines for membrane fusion. Nat Rev Mol Cell
882 Biol. 2006;7: 631–643. doi:10.1038/nrm2002
883 61. Pirooz SD, He S, Zhang T, Zhang X, Zhao Z, Oh S, et al. UVRAG is required for
884 virus entry through combinatorial interaction with the class C-Vps complex and SNAREs.
885 Proc Natl Acad Sci U S A. 2014;111: 2716–2721. doi:10.1073/pnas.1320629111
886 62. Langston PK, Nambu A, Jung J, Shibata M, Aksoylar HI, Lei J, et al. Glycerol
887 phosphate shuttle enzyme GPD2 regulates macrophage inflammatory responses. Nat
888 Immunol. 2019;20: 1186–1195. doi:10.1038/s41590-019-0453-7
889 63. Schoggins JW. Interferon-Stimulated Genes: What Do They All Do? Annual Review
890 of Virology. 2019;6: 567–584. doi:10.1146/annurev-virology-092818-015756
891 64. Tartour K, Nguyen XN, Appourchaux R, Assil S, Barateau V, Bloyet LM, et al.
892 Interference with the production of infectious viral particles and bimodal inhibition of
893 replication are broadly conserved antiviral properties of IFITMs. PLoS Pathog. 2017;13:
894 e1006610. doi:10.1371/journal.ppat.1006610
895 65. García-Sastre A. Ten Strategies of Interferon Evasion by Viruses. Cell Host Microbe.
896 2017;22: 176–184. doi:10.1016/j.chom.2017.07.012
897 66. Schulz KS, Mossman KL. Viral Evasion Strategies in Type I IFN Signaling – A
898 Summary of Recent Developments. Front Immunol. 2016;7. doi:10.3389/fimmu.2016.00498
899 67. Schoggins JW, Macduff DA, Imanaka N, Gainey MD, Shrestha B, Eitson JL, et al.
900 Pan-viral specificity of IFN-induced genes reveals new roles for cGAS in innate immunity.
901 Nature. 2013. doi:10.1038/nature12862
902 68. Taylor HE, Khatua AK, Popik W. The innate immune factor apolipoprotein L1
903 restricts HIV-1 infection. J Virol. 2014;88: 592–603. doi:10.1128/JVI.02828-13
904 69. Yamane D, Feng H, Rivera-Serrano EE, Selitsky SR, Hirai-Yuki A, Das A, et al.
905 Basal expression of interferon regulatory factor 1 drives intrinsic hepatocyte resistance to
906 multiple RNA viruses. Nat Microbiol. 2019;4: 1096–1104. doi:10.1038/s41564-019-0425-6
907 70. Burke JE, McPhail JA, Rathinaswamy M, Jenkins ML. Defining how viruses
908 manipulate lipid phosphoinositides through activation of PI4P kinases to mediate viral
909 replication. The FASEB Journal. 2020;34: 1–1. doi:10.1096/fasebj.2020.34.s1.02060
910 71. Gillespie LK, Hoenen A, Morgan G, Mackenzie JM. The Endoplasmic Reticulum
911 Provides the Membrane Platform for Biogenesis of the Flavivirus Replication Complex.
912 Journal of Virology. 2010;84: 10438–10447. doi:10.1128/JVI.00986-10
913 72. Olias P, Etheridge RD, Zhang Y, Holtzman MJ, Sibley LD. Toxoplasma Effector
914 Recruits the Mi-2/NuRD Complex to Repress STAT1 Transcription and Block IFN-γ-
915 Dependent Gene Expression. Cell Host Microbe. 2016;20: 72–82.

916 doi:10.1016/j.chom.2016.06.006
917 73. Nusinzon I, Horvath CM. Interferon-stimulated transcription and innate antiviral
918 immunity require deacetylase activity and histone deacetylase 1. PNAS. 2003;100: 14742–
919 14747. doi:10.1073/pnas.2433987100
920 74. Vlasáková J, Nováková Z, Rossmeislová L, Kahle M, Hozák P, Hodný Z. Histone
921 deacetylase inhibitors suppress IFNα-induced up-regulation of promyelocytic leukemia
922 protein. Blood. 2007;109: 1373–1380. doi:10.1182/blood-2006-02-003418
923 75. Saleem MA, O'Hare MJ, Reiser J, Coward RJ, Inward CD, Farren T, et al. A
924 conditionally immortalized human podocyte cell line demonstrating nephrin and podocin
925 expression. J Am Soc Nephrol. 2002;13: 630–638. doi:10.1681/ASN.V133630
926 76. Nakabayashi H, Taketa K, Miyano K, Yamane T, Sato J. Growth of human hepatoma
927 cells lines with differentiated functions in chemically defined medium. Cancer Res. 1982;42:
928 3858–3863.
929 77. Buchrieser J, Dufloo J, Hubert M, Monel B, Planas D, Rajah MM, et al. Syncytia
930 formation by SARS-CoV-2-infected cells. EMBO J. 2021;40: e107405.
931 doi:10.15252/embj.2020107405
932 78. Chazal M, Beauclair G, Gracias S, Najburg V, Simon-Loriere E, Tangy F, et al. RIG-I
933 Recognizes the 5' Region of Dengue and Zika Virus Genomes. Cell Rep. 2018;24: 320–328.
934 doi:10.1016/j.celrep.2018.06.047
935 79. Boukadida C, Marnata C, Montserret R, Cohen L, Blumen B, Gouttenoire J, et al. NS2
936 proteins of GB virus B and hepatitis C virus share common protease activities and membrane
937 topologies. J Virol. 2014;88: 7426–44. doi:10.1128/JVI.00656-14
938 80. Wakita T, Pietschmann T, Kato T, Date T, Miyamoto M, Zhao Z, et al. Production of
939 infectious hepatitis C virus in tissue culture from a cloned viral genome. Nat Med. 2005;11:
940 791–6. doi:10.1038/nm1268
941 81. Kaul A, Woerz I, Meuleman P, Leroux-Roels G, Bartenschlager R. Cell culture
942 adaptation of hepatitis C virus and in vivo viability of an adapted variant. J Virol. 2007;81:
943 13168–79. doi:10.1128/JVI.01362-07
944 82. Aicher S, Kakkanas A, Cohen L, Blumen B, Oprisan G, Njouom R, et al. Differential
945 regulation of the Wnt/beta-catenin pathway by hepatitis C virus recombinants expressing core
946 from various genotypes. Sci Rep. 2018;8: 11185. doi:10.1038/s41598-018-29078-2
947 83. Malo N, Hanley JA, Cerquozzi S, Pelletier J, Nadon R. Statistical practice in high-
948 throughput screening data analysis. Nat Biotechnol. 2006;24: 167–175. doi:10.1038/nbt1186
949 84. Birmingham A, Selfors LM, Forster T, Wrobel D, Kennedy CJ, Shanks E, et al.
950 Statistical Methods for Analysis of High-Throughput RNA Interference Screens. Nat
951 Methods. 2009;6: 569–575. doi:10.1038/nmeth.1351
952 85. McQuin C, Goodman A, Chernyshev V, Kamentsky L, Cimini BA, Karhohs KW, et
953 al. CellProfiler 3.0: Next-generation image processing for biology. PLOS Biology. 2018;16:
954 e2005970. doi:10.1371/journal.pbio.2005970
955 86. Mutso M, Saul S, Rausalu K, Susova O, Žusinaite E, Mahalingam S, et al. Reverse
956 genetic system, genetically stable reporter viruses and packaged subgenomic replicon based
957 on a Brazilian Zika virus isolate. J Gen Virol. 2017;98: 2712–2724. doi:10.1099/jgv.0.000938
958 87. Schwarz MC, Sourisseau M, Espino MM, Gray ES, Chambers MT, Tortorella D, et al.
959 Rescue of the 1947 Zika Virus Prototype Strain with a Cytomegalovirus Promoter-Driven
960 cDNA Clone. mSphere. 2016;1. doi:10.1128/mSphere.00246-16
961

962

963

964 **Figure legends**

965

966 **Figure 1**. **A loss of function screen identified genes modulating ZIKV replication in IFN-**
967 **stimulated human microglial cells**. (A) Scheme summarizing the screen conditions. (B, C) Scatter
968 plots showing the rZ-score obtained in the 1st (B) and second analysis (C) of the 2 screens. The green
969 line represents the linear regression, as compared to the expected perfect correlation (dotted black line).
970 Antiviral and proviral hits are depicted in red and blue, respectively. (D) List of the antiviral and proviral
971 hits as identified by the 2 analysis of the 2 screens. Assessment of the antiviral (E, F) and proviral (G,
972 H) activities of some hits. HMC3 cells were transfected with either pool of 3 siRNAs against the
973 indicated candidate gene or non-targeting (NT) siRNAs, treated with IFNα2 (200U/mL) for 24 hours
974 and infected with ZIKV (at an MOI of 5 PFU/cell) for 24 hours. Control cells transfected with NT
975 siRNA in the absence of IFNα2 treatment (NT-IFN) are included. (E, G) Cell-associated viral RNA was
976 quantified by RT-qPCR and expressed as genome equivalents (GE) per µg of total cellular RNA. (F, H)
977 The number of cells positive for viral protein E was assessed by flow cytometry and are expressed
978 relatively to the NT+IFN control of each experiment. Data are means ± SD of three or four independent
979 experiments, *p<0.05, **p<0.01,***p<0.001, paired t-tests.

980

981 **Figure 2. Effect of a selection of candidate genes on HCV and SARS-CoV-2 replication. (**A-D).
982 Huh-7.5 cells were transfected with a pool of 3 siRNAs against selected candidates (antiviral and
983 proviral genes, as identified in the ZIKV screen (Fig. 1), are in red and blue, respectively) or non-
984 targeting (NT) siRNAs, treated with IFNα2 (200U/mL) for 24 hours, then infected with HCV at a MOI
985 of 3 TCID50/cell for 48 hours. (A, C) Cell-associated viral RNA was quantified by RT-qPCR and
986 expressed as genome equivalents (GE) per µg of total cellular RNA. (B, D) Release of infectious HCV
987 particles was determined by TCID50 assays. Data are expressed relatively to the NT+IFN control of
988 each experiment. Plotted values are expressed relative to mean NT+IF across experiements and
989 represent means ± SD of two independent experiments each in duplicates, *p<0.05,
990 **p<0.01,***p<0.001, ****p<0.0001 paired t-tests. (E-H). A549-ACE2 cells were transfected with a
991 pool of 3 siRNAs against selected candidates (antiviral genes in red, proviral genes in blue) or non-
992 targeting (NT) siRNAs, treated with IFNα2 (200U/mL) for 24 hours and infected with SARS-CoV-2 at
993 a MOI of 2 for 24 hours. (E, G) Cell-associated viral RNA was quantified by RT-qPCR and expressed
994 as genome equivalents (GE) per µg of total cellular RNA. (F, H) The number of cells positive for the
995 viral protein spike (S) was assessed by flow cytometry Data are expressed relatively to the NT+IFN
996 control of each experiment. Data are means ± SD of triplicates of one experiment, *p<0.05,
997 **p<0.01,***p<0.001, paired t-tests.

998

999 **Figure 3. Effect of reduced expression of APOL1 and APOL3 on the replication of a panel of**
1000 **viruses in HMC3 cells and podocytes.** (A, E) *APOL1* mRNA and *APOL3* mRNA abundance were
1001 quantified by RT-qPCR analysis in HMC3 cells or podocytes treated or not with IFNα2 (200U/mL) for
1002 24 hours and expressed as copy numbers per μg of total cellular RNA. HMC3 cells (B) or podocytes (F)
1003 were transfected with pool of 3 siRNAs targeting *APOL1, APOL3* and *USP18* mRNAs or with non-
1004 targeting (NT) control siRNAs. The relative amounts of *APOL1, APOL3* and *USP18* mRNAs were
1005 determined by RT-qPCR analysis and were normalized to that of GAPDH mRNA. They are expressed
1006 as compared to abundance relative to cells transfected with control NT siRNAs. HMC3 cells (C) or
1007 podocytes (G) were transfected with the indicated siRNAs, treated, or not, with IFNa2 (200U/mL) for
1008 24 hours, and infected with ZIKV for 24 hours. HMC3 cells were infected at a MOI of 2 and podocytes
1009 at a MOI of 1. The percentages of cells that were positive for the viral E proteins were determined by
1010 flow cytometric analysis. Data are expressed relatively to the siRNA NT control of each experiment.
1011 HMC3 cells (D) or podocytes (H) were treated with IFNα2 (200U/mL), transfected with the indicated
1012 siRNAs pools and subjected to Western blotting analysis with antibodies against the indicated proteins.
1013 (I) HMC3 cells were transfected with the indicated siRNAs pools, treated with IFNa2 (200U/mL) for
1014 24 hours and infected with the indicated viruses for 18 to 24 hours, at the MOI indicated in the MM
1015 section. The percentages of the cells positive for viral proteins or GFP were determined by flow
1016 cytometric analysis. Data are means ± SD of three or four independent experiments, *p<0.05,
1017 **p<0.01,***p<0.001, paired t-tests.
1018
1019 **Figure 4. APOL1 and APOL3 promote viral replication independently of their interaction with**
1020 **phosphoinositides**. HMC3 cells were transfected with GFP-tagged versions of APOL1 and APOL3.
1021 Thirty hours later, they were stained with antibodies recognizing GM130 (A) or PI4KB (B) and with
1022 NucBlue to detect nuclei. Images are representative of numerous observations over 2 independent
1023 experiments. The white arrow shows an APOL1-GFP-positive vesicle. (C) HCM3 cells were treated
1024 with different concentrations of the PI4KB inhibitor and were stained for PI(4)P. (D) HMC3 cells treated
1025 with different doses of PI4KB inhibitor were infected with CVB3, WNV or ZIKV, in the presence or
1026 absence of IFNα2 (200U/mL). The percentages of the cells positive for viral proteins were determined
1027 by flow cytometric analysis. Data are means ± SD of three independent experiments, *p<0.05,
1028 **p<0.01,***p<0.001, one-way ANOVA.
1029

1030 **Figure 5. MTA2 restricts ZIKV replication in IFNα2-stimulated cells.** HMC3 (A, B, E, F, I) and
1031 Huh-7 cells (C, D, G, H, J) were transfected with pool of 3 siRNAs targeting *MTA2* or *IFNAR1* mRNAs
1032 or non-targeting (NT) control siRNAs, treated or not with IFNα2 (100U/mL) for 24 hours, and infected
1033 with ZIKV (MOI of 1 for HMC3 cells, MOI of 5 for Huh-7 cells) for 24 hours. (A-D) The relative
1034 amounts of *MTA2* and *IFNAR1* mRNAs were determined by RT-qPCR analysis and normalized to that

1035 of *GAPDH* mRNA and siRNA-NT without IFN. (E, G) Cell-associated viral RNA was quantified by
1036 RT-qPCR and expressed as genome equivalents (GE) per µg of total cellular RNA. (F, H) Number of
1037 infected cells was assessed by staining of viral protein E and flow cytometry analysis. (I, J) Cells were
1038 treated with IFNα2 (200U/mL) or left untreated, transfected with the indicated siRNAs pools and
1039 subjected to Western blotting analysis with antibodies against the indicated proteins. Data are means ±
1040 SD of three independent experiments, *p<0.05, **p<0.01,***p<0.001, paired t-tests.

1041

1042 **Figure 6. Effect of reduced expression of MTA2 on the replication of YFV, WNV, VSV and MeV-**
1043 **GFP.** Huh-7 cells were transfected with the indicated siRNAs pool, treated or not with IFNα2
1044 (200U/mL) for 24 hours and infected with WNV (A) or YFV (B) for 24 hours, at the MOIs indicted in
1045 the MM section. The percentages of the cells positive for viral protein Env was determined by flow
1046 cytometric analysis. HMC3 cells were transfected with the indicated siRNAs pool, treated or not with
1047 IFNα2 (200U/mL) for 24 hours and infected with VSV for 18 hours (C) or MeV-GFP for 24 hours (D),
1048 at the MOIs indicted in the MM section. The percentages of the cells positive for viral protein G or GFP
1049 were determined by flow cytometric analysis. Data are expressed relatively to the siRNA NT control of
1050 each experiment. Data are means ± SD of three or four independent experiments, *p<0.05,
1051 **p<0.01,***p<0.001, paired t-tests.

1052

1053 **Supplementary figure legends**

1054

1055 **Figure S1. Quality control and reproducibility of the screens.** (A) HMC3 cells were transfected with
1056 either pool of 3 siRNAs against IFNAR or IFITM3 or non-targeting (NT) siRNAs, treated with IFNα2
1057 (1000U/mL) for 24 hours and infected with ZIKV PF13 at a MOI of 7 PFU/cell for 24 hours. The
1058 number of cells positive for viral protein E was assessed by confocal analysis using the pan-flavivirus
1059 anti-E antibody 4G2. (B) Distribution of the "number of cells per 3 fields" parameter for each screen.
1060 The values of the control wells (cells transfected with siRNA targeting KIF11) are shown in dark gray.
1061 (C) Representation of the number of cells per 3 fields of screen 1 as a function of the screen 2. The green
1062 line represents the linear regression as compared to the expected perfect correlation (dotted black line).
1063 (D) Distribution of the "percentage of infected cells" parameter for each screen in the first analysis. The
1064 values of the control conditions (cells transfected with siRNAs targeting IFNAR1 or IFNAR2) are
1065 shown in dark grey. (E) Representation of the percentage of infected cells per well of screen 1 as a
1066 function of screen 2, as identified by the first analysis. The green line represents the linear regression as
1067 compared to the expected perfect correlation (dotted black line). (F) Representation of the percentage
1068 of infected cells per well in the analysis 1 as a function of analysis 2. The green line represents the linear
1069 regression. (G) HMC3 cells were transfected with pools of 3 siRNAs targeting the indicated genes or

1070 with non-targeting (NT) control siRNAs. The relative abundances of the mRNAs of the candidate genes
1071 were determined by RT-qPCR analysis and were normalized with respect to GAPDH mRNA level.
1072 They are expressed relatively to abundance in cells transfected with NT siRNAs set at 1. Data are means
1073 ± SD of three or four independent experiments. ND: not determined due to mRNA levels below assay
1074 threshold. The samples are the same than in Fig. 1E-H.
1075
1076 **Figure S2. Efficacy of the specific siRNAs.** Huh-7.5 cells (A) or A549-ACE2 cells (B) were transfected
1077 with pool of 3 siRNAs targeting the indicated genes or with non-targeting (NT) control siRNAs. The
1078 relative abundances of the mRNAs of the candidate genes were determined by RT-qPCR analysis and
1079 were normalized with respect to GAPDH mRNA level. Values are expressed relatively to abundance in
1080 cells transfected with NT siRNA in each experiment, set at 1. Data are means ± SD of three or four
1081 independent experiments. ND: not determined due to mRNA levels below assay threshold. The samples
1082 are the same than in Fig. 2.
1083
1084 **Figure S3. Localization of GFP-tagged version of APOL1 and APOL3 in HMC3 cells**. Cells were
1085 transfected with GFP-tagged versions of APOL1 and APOL3. Thirty hours later, they were stained with
1086 antibodies recognizing EEA1 or CD63 and with NucBlue to detect nuclei. Images are representative of
1087 numerous observations over 2 independent experiments.

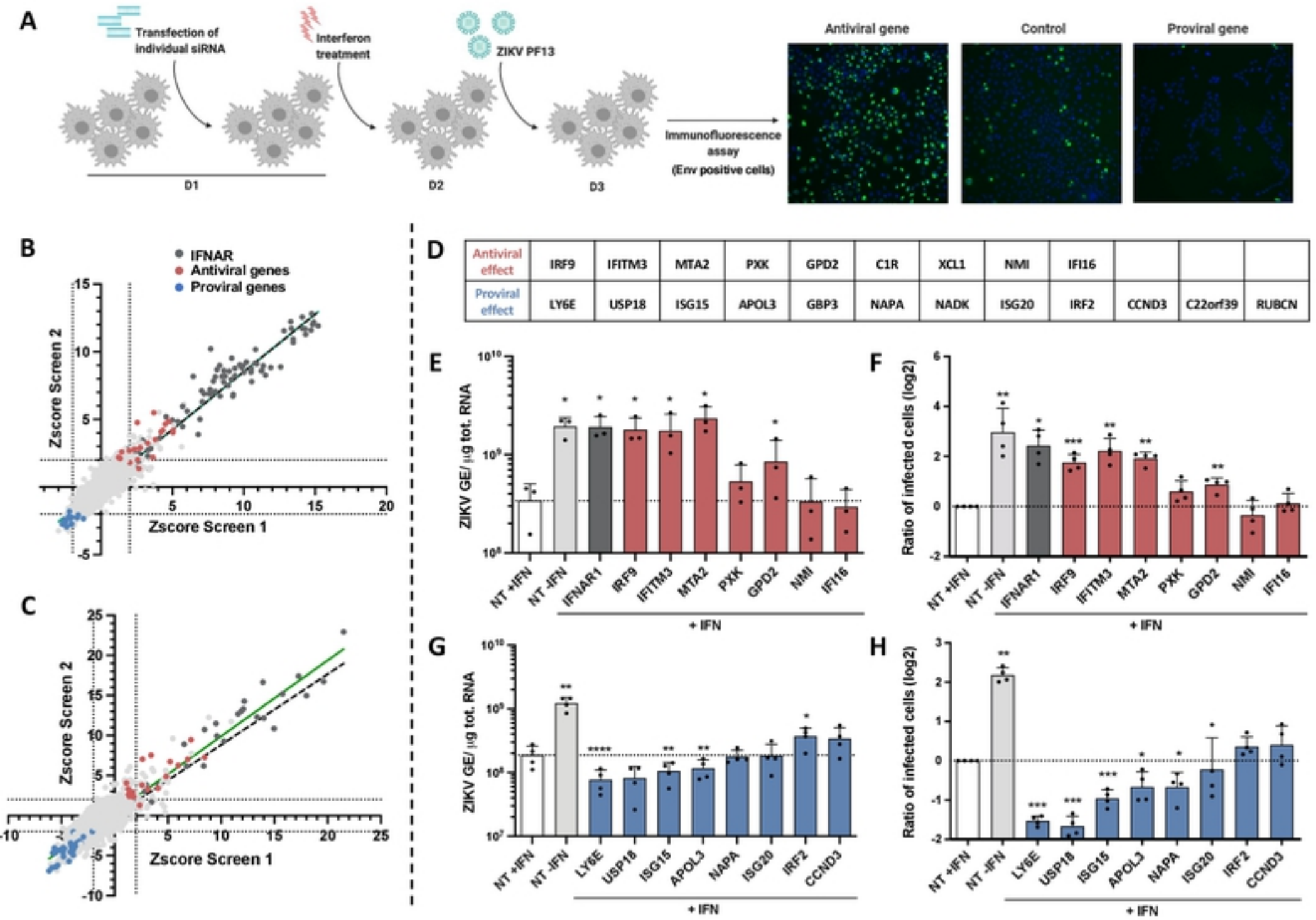
A
Transfection of individual siRNA
Interferon treatment
ZIKV PF13
D1
D2
D3
Immunofluorescence assay (Env positive cells)
Antiviral gene
Control
Proviral gene
B
IFNAR
Antiviral genes
Proviral genes
Zscore Screen 2
Zscore Screen 1
C
Zscore Screen 2
Zscore Screen 1
D
Antiviral effect | IRF9 | IFITM3 | MTA2 | PXK | GPD2 | C1R | XCL1 | NMI | IFI16
Proviral effect | LY6E | USP18 | ISG15 | APOL3 | GBP3 | NAPA | NADK | ISG20 | IRF2 | CCND3 | C22orf39 | RUBCN
E
ZIKV GE/ µg tot. RNA
NT +IFN
NT -IFN
IFNAR1
IRF9
IFITM3
MTA2
PXK
GPD2
NMI
IFI16
+ IFN
F
Ratio of infected cells (log2)
G
ZIKV GE/ µg tot. RNA
LY6E
USP18
ISG15
APOL3
NAPA
ISG20
IRF2
CCND3
H
Ratio of infected cells (log2)

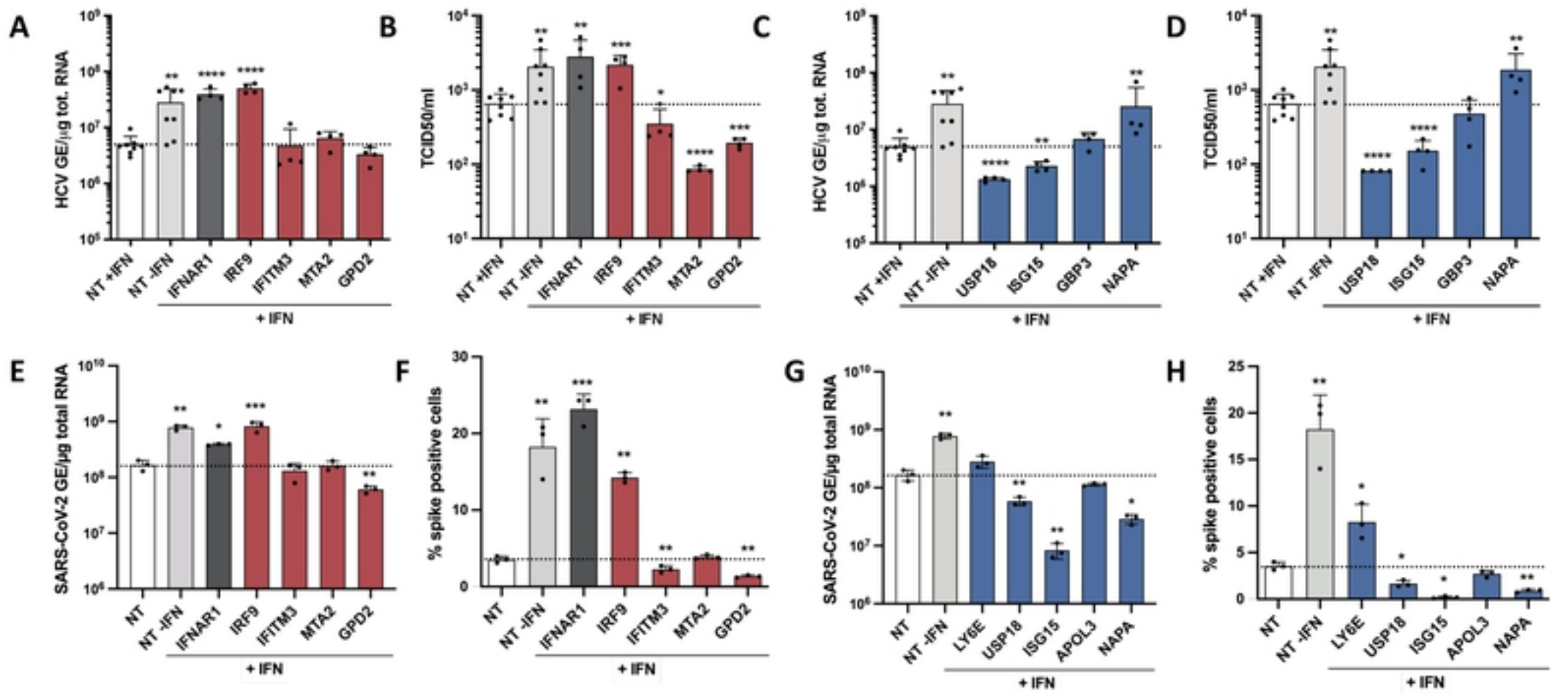
A
HCV GE/µg tot. RNA
NT +IFN
NT -IFN
IFNAR1
IRF9
IFITM3
MTA2
GPD2
+ IFN
B
TCID50/ml
C
USP18
ISG15
GBP3
NAPA
D
E
SARS-CoV-2 GE/µg total RNA
NT
F
% spike positive cells
G
LY6E
APOL3
H

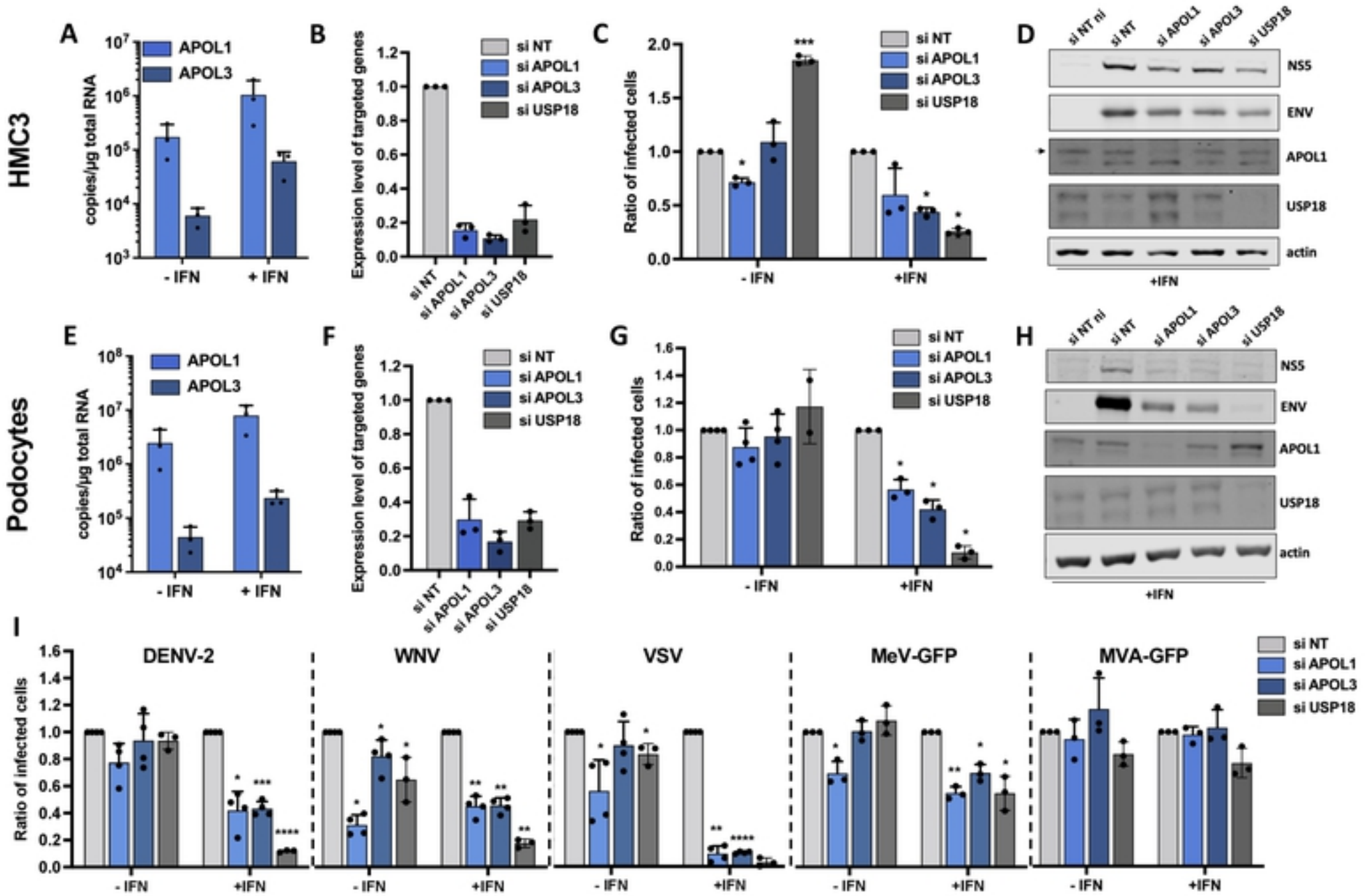
HMC3
Podocytes
A
B
C
D
E
F
G
H
I
APOL1
APOL3
copies/µg total RNA
- IFN
+ IFN
Expression level of targeted genes
si NT
si APOL1
si APOL3
si USP18
Ratio of infected cells
si NT ni
NS5
ENV
actin
DENV-2
WNV
VSV
MeV-GFP
MVA-GFP

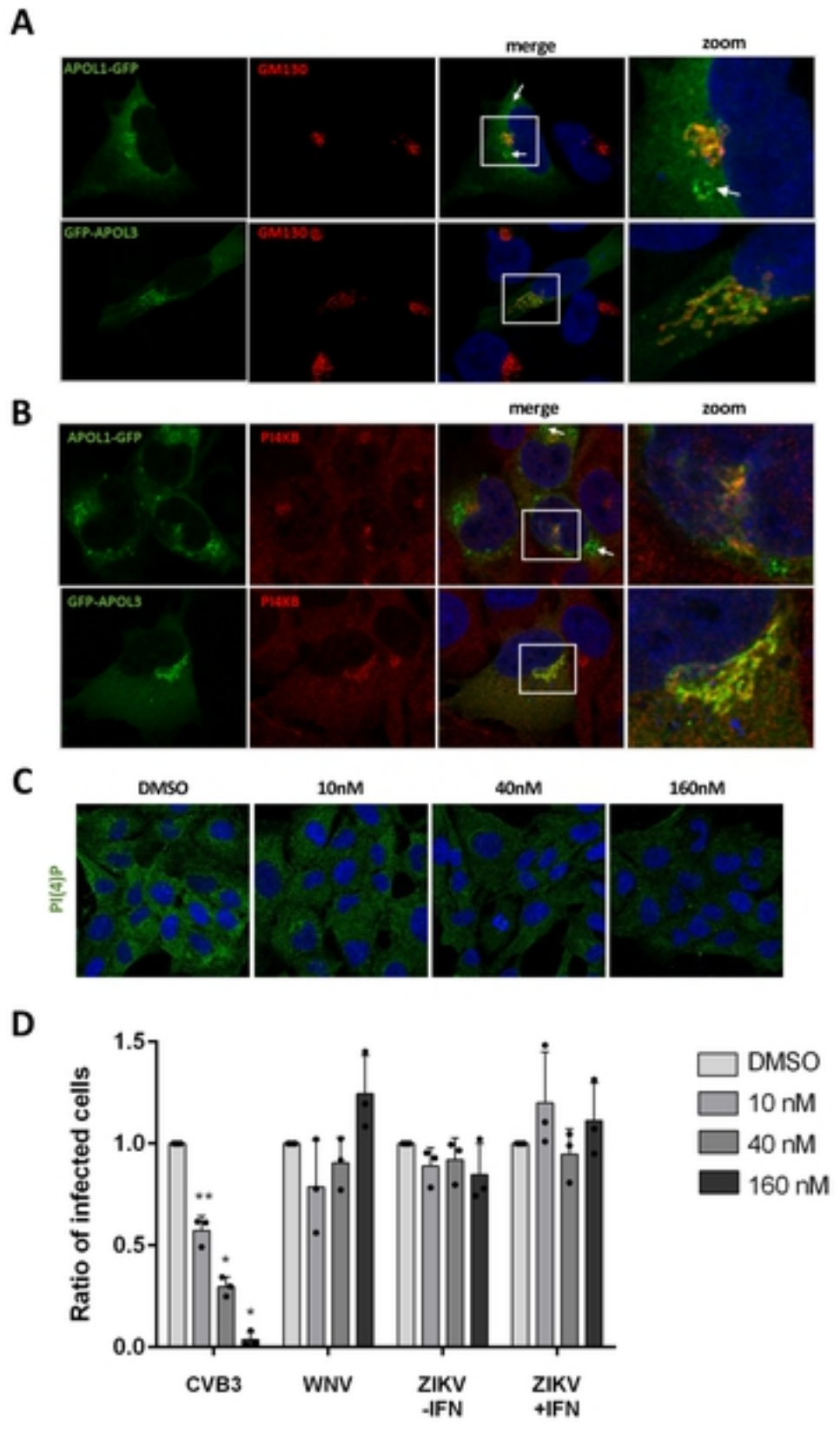
A
merge
zoom
APOL1-GFP
GM130
GFP-APOL3
GM130
B
merge
zoom
APOL1-GFP
PI4KB
GFP-APOL3
PI4KB
C
DMSO
10nM
40nM
160nM
PI(4)P
D
Ratio of infected cells
1.5
1.0
0.5
0.0
CVB3
WNV
ZIKV -IFN
ZIKV +IFN
DMSO
10 nM
40 nM
160 nM

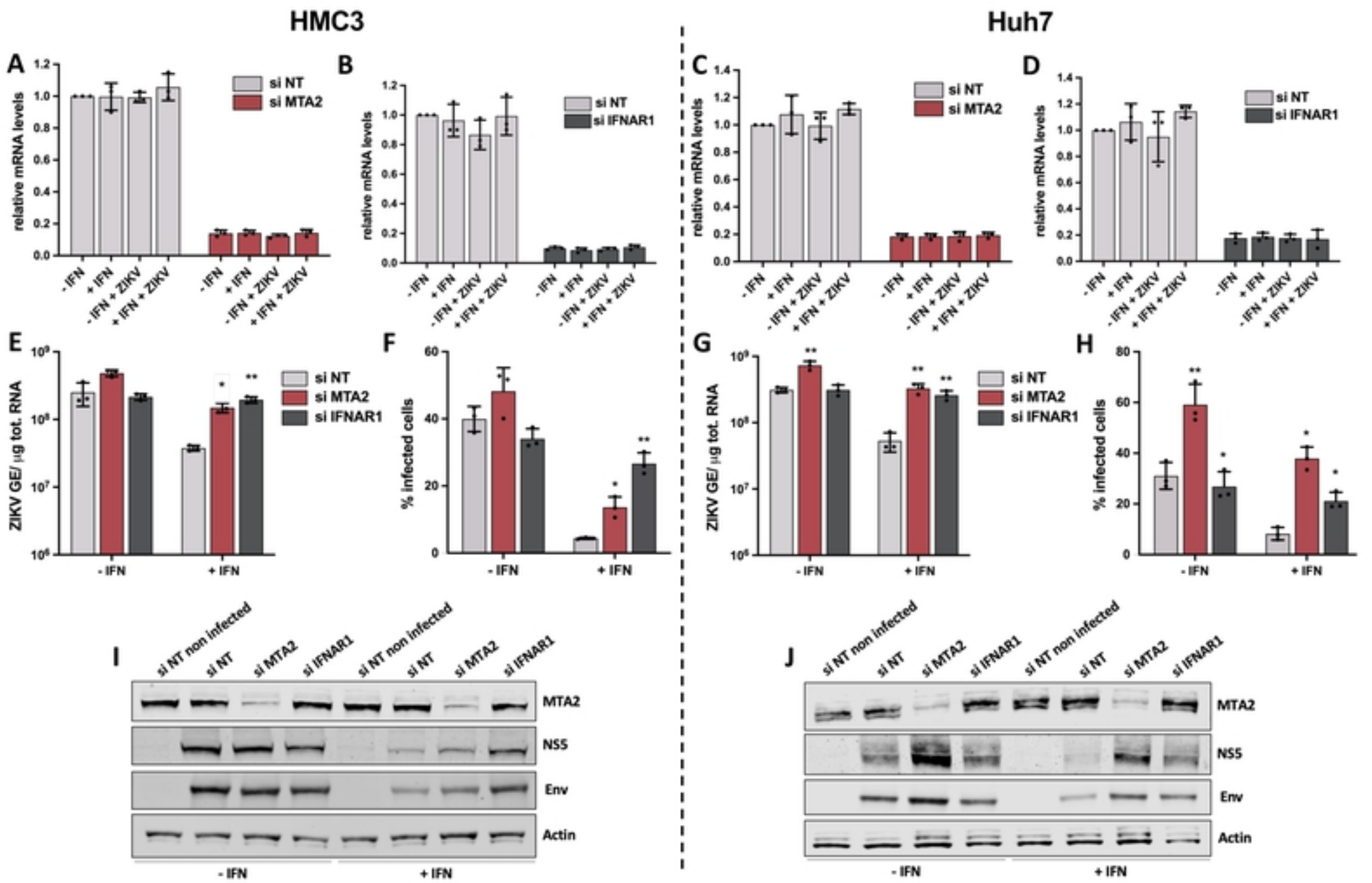
HMC3
Huh7
A
B
C
D
relative mRNA levels
si NT
si MTA2
si IFNAR1
- IFN
+ IFN
- IFN + ZIKV
+ IFN + ZIKV
E
F
G
H
ZIKV GE/ µg tot. RNA
% infected cells
I
J
si NT non infected
MTA2
NS5
Env
Actin

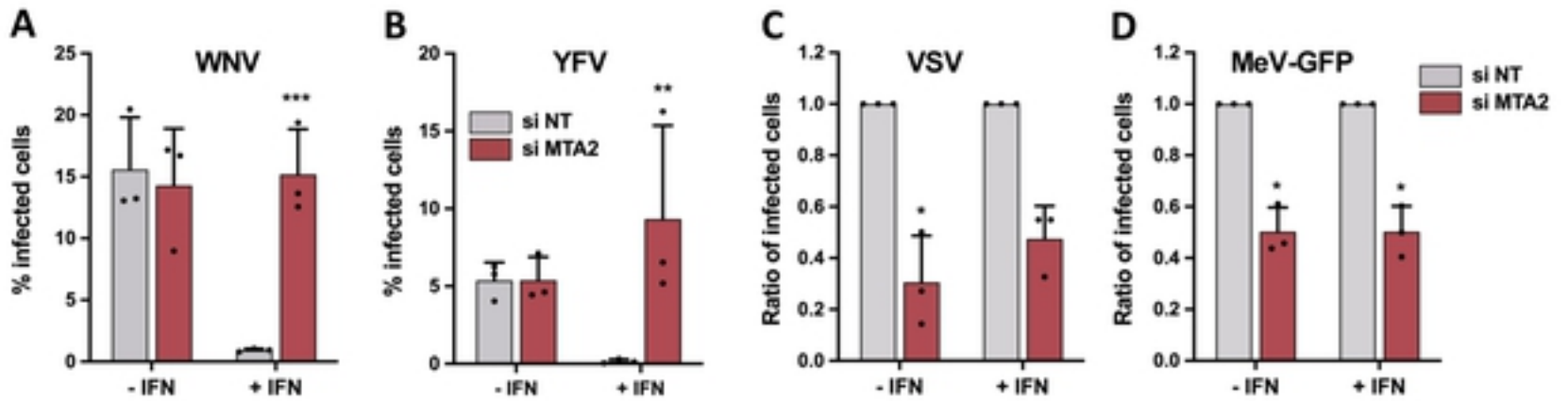
A
WNV
% infected cells
25
20
15
10
5
0
***
- IFN
+ IFN
B
YFV
% infected cells
20
15
10
5
0
si NT
si MTA2
**
- IFN
+ IFN
C
VSV
Ratio of infected cells
1.2
1.0
0.8
0.6
0.4
0.2
0.0
*
- IFN
+ IFN
D
MeV-GFP
Ratio of infected cells
1.2
1.0
0.8
0.6
0.4
0.2
0.0
si NT
si MTA2
*
*
- IFN
+ IFN